Planar Simulation of Bubble Growth in Film Boiling Using a Variant of VOF Method

By

Deepak Kumar Agarwal

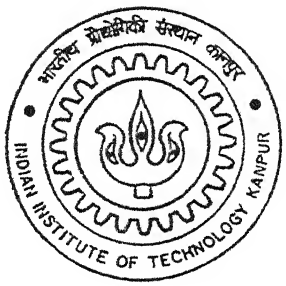

DEPARTMENT OF MECHANICAL ENGINEERING

Indian Institute of Technology, Kanpur

MAY, 2004

Planar Simulation of Bubble Growth in Film Boiling Using a Variant of VOF Method

A Thesis Submitted
in Partial Fulfilment of the Requirements
for the Degree of

Master of Technology

by

Deepak Kumar Agarwal

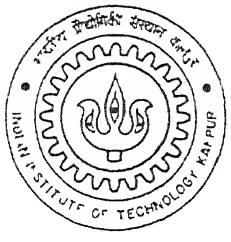

to the

DEPARTMENT OF MECHANICAL ENGINEERING
INDIAN INSTITUTE OF TECHNOLOGY KANPUR
INDIA

May, 2004

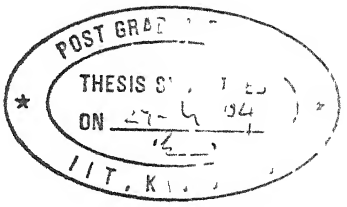

Certificate

It is certified that the work contained in the thesis entitled **Planar Simulation of Bubble Growth in Film Boiling Using a Variant of VOF Method** by **Deepak Kumar Agarwal**, has been carried out under my supervision and that this work has not been submitted elsewhere for a degree

Gautam Biswas
Dr Gautam Biswas
Professor
Department of Mechanical Engineering
Indian Institute of Technology Kanpur
Kanpur-208016, India

May, 2004

To
my father, mother
and sisters

Acknowledgements

I express my whole-hearted gratitude, deep regards and thanks to my thesis supervisor Prof G Biswas for his excellent supervision, invaluable suggestions and generous help I was deeply impressed by his meticulousness, systematic approach and above all total devotion to his work It is due to his excellent guidance, consistent inspiration, encouragement and confidence in me that I have made it He is a special supervisor who treats his students like his close friends and helps them in all possible ways quite generously I always possessed a deep admiration towards his kind-hearted and amicable personality and feel very fortunate to get him as my thesis supervisor

I am extremely thankful to Mr Abhinandan Agrawal for his valuable inputs at the begning of my thesis work I am glad to record my thanks to my colleagues in CFD Lab who made my working here a pleasant and memorable one With Daniel Gerlach, and Garuav Tomar I had many useful discussions on programming and code development They helped me in all possible ways while working with different problems of my thesis They also helped me in programming and postprocessing I am also thankful to co-researchers, namely Shaligram Tiwari, Arul Prakash, Somnath Roy, Santanu De, Amaresh, Akshika Maheshwari, Shubhankar and Siddhartha Pal I am also extremely grateful to my friends Ankit, Aprajita, Akshika and Rakhi for their continuous and everlasting support I extend my thanks to Ms Neetu Srivastava who helped me in word processing

Once again, I would like to thank all my classmates for their smile and friendship making the life at I I T Kanpur enjoyable and memorable

Last but not least, the silent support, good wishes and blessings of my parents and other family members have been the source of my inspiration throughout my research work Special thanks also go to my beloved fiancee Payal for her encouragement, support, patience and love

Deepak Kumar Agarwal

Abstract

A planar simulation of film boiling and bubble formation in water at 373°C, 219 bar on an isothermal horizontal surface was performed by using a volume of fluid (VOF) based interface tracking method The complete Navier-Stokes equations and thermal energy equations were solved in conjunction with a interface mass transfer model The numerical method takes into account the effect of temperature on the transportive thermal properties (thermal conductivity and specific heat) of vapor, effects of surface tension, the interface mass transfer and the corresponding latent heat The computations provided a good insight into film boiling yielding quantitative information on unsteady periodic bubble release patterns and on the spatially and temporally varying film thickness The computations also predicted the transport coefficients on the horizontal surface, which were greatly influenced by the variations in fluid properties, compared to calculations with constant properties

Contents

Certificate ii

Dedication iii

Abstract iv

Contents vi

List of Figures viii

List of Tables x

Nomenclature xi

1 Introduction 1

1 1 Description of the Problem 2

1 2 Scope of the Present Work 2

1 3 Layout of the Thesis 3

2 Review of Literature 4

2 1 Review of Boiling Flows 4

2 2 Overview of Methods for Simulation of Free Surface Flows 5

2 3 Epilogue 9

3 Formulation of the Problem 10

3 1 Governing Equations 10

3 2 Boundary Conditions 11

3 3 Interface Tracking 12

3 3 1 Least Squares Interface Reconstruction Algorithm (LVIRA) 13

3 3 2 Direction Split Approach 14

3 4 Jump Conditions at Liquid Vapor Interface 16

3 5 Modified Momentum Equation 18

3 6 Smoothing of the Void Field 18

3 7 Numerical Procedure 20

4 Results and Discussion 22

5 Conclusion and Scope for Future Work 47

References 49

A 53

A 1 List of Subroutines 53

A 2 Flow Chart 54

List of Figures

2 1 A true interface, and the corresponding void field Reconstruction of the interface by horizontal or vertical lines (SLIC) and by straight lines of arbitrary inclination (PLIC) 8

3 1 The domain for the simulation of film boiling 11

3 2 A typical two phase cell with piecewise linear interface 13

3 3 Schematic of cell flux calculation 15

4 1 Bubble interface for three different grid resolutions 23

4 2 Bubble interface for two different time steps Grid resolution is kept as 180×360 . 24

4 3 Bubble release from the constant wall temperature surface for two complete cycles 28

4 4 Fluctuation of space averaged heat flux on the wall surface with constant fluid thermal properties 30

4 5 Fluctuation of space averaged heat flux on the wall surface with variable fluid thermal properties 30

4 6 Fluctuation of liquid-vapor interface heat flux with time 31

4 7 Variation of fractional vapor volume with time for constant and variable thermal properties 32

4 8 Isotherms for a superheat of $\Delta\theta = 15°C$ in the vapor over the computational domain at time instants 0 375 s and 0 625 s respectively In (b) contour levels are spaced at a temperature difference of $1°C$ for a range between $647 - 658°C$ 34

4 9 Isotherms for a superheat of $\Delta\theta = 15°C$ in an enlarged region of Fig 11(a) near the location of minimum film thickness 35

4 10 Variation of peak heat flux value with the reciprocal of minimum film thickness at various time instants 36

4 11 Velocity vectors for a superheat of $\Delta\theta = 15°$ at time = 0 375 s 37

4 12 Velocity vectors for a superheat of $\Delta\theta = 15°$ at time = 0 625 s 38

4 13 Streamlines at time = 0 375 s . 39

4 14 Streamlines at time = 0 625 s . . 40

4 15 Variation of heat flux on the wall surface at various time instants before bubble release on right symmetric boundary . . 41

4 16 Variation of heat flux on wall surface at time instants after the bubble release on right symmetric boundary . 42

4 17 Nusselt number variation with time (with constant thermal properties) 43

4 18 Nusselt number variation with time (with variable thermal properties) 44

List of Tables

4 1	Properties from NBS/NRC table for vapor phase	25
4 2	Properties used for constant property simulation	25
4 3	Interfacial properties and density	25
4 4	Comparison of predicted Nusselt number with that of Berenson and Klimenko correlation for constant and variable thermal properties	46

Nomenclature

c_p, c_v	specific heat at constant pressure/ volume
Gr	Grashop number
g	gravitational acceleration
H	height of computational domain
h_{lg}	latent heat of vaporization
k	thermal conductivity´
l	offset length from cell center to the linear interface
$\bar{N}_u$	space averaged Nusselt number
n	interface normal vector, pointing into liquid phase
P_o	saturation pressure in excess of hydrostatic pressure
Pr	Prandtl number
p	total pressure (Pa or in bar)
q	heat flux vector
S_c	surface boundary the computational cell
S_I	phase interface surface
t	time
u	x component of velocity
U_i, U_j	velocity vectrs
V	volume
V_c	cell volume

v	y component of velocity
$\mathbf{v}$	fluid velocity
x	spatial coordinate in the horizontal direction
x_i, x_j	space vectors
y	spatial coordinate in the vertical direction

Greek

α	cell void fraction
$\tilde{\alpha}$	smoothing void fraction
β	Jakob number
δ	initial interface height from solid wall
δt	time increment
κ	curvature
λ	chracteristic length
λ_0	Taylor fastest growing wavelength
μ	dynamic viscosity
ρ	density
σ	surface tension
θ	temperature
$\Delta\theta$	degree of superheat

Subscripts

i	interface
l	liquid phase
sat	saturation condition
sup	superheated
g	vapor phase

Superscripts

n	values at old time step
$n+1$	values at new time step

Chapter 1

Introduction

Boiling flows are ubiquitous in the energy and processing industries due to the fact that phase change processes are an efficient way of transporting energy Many aspects of boiling flows that are not well understood even today. The small spatial scales and fast time constants of many of the physical processes associated with the boiling are the impediments of reliable experimental data Advanced computational methods are capable of providing solutions for fluid flow problems with moving interfaces separating gas and liquid phases

The phase change problems are dependent on the simultaneous coupling of many effects most of them can not be ignored The modeling of mass, momentum and energy transport must include surface tension, latent heat, interphase mass transfer, discontinuous material properties and complicated liquid-vapor interface dynamics Here in this work we have included all these properties while predicting and analyising the formation of vapor bubbles in film boiling region

1.1 Description of the Problem

Film boiling is characterized by the existence of a continuous vapor film between a heated surface and the liquid layer In this work, the bubble formation and heat transfer on a horizontal surface have been numerically analyzed using a volume of fluid (VOF) based interface tracking method For this, we consider a heated wall with a uniform temperature of 388° C, superheated by 15° C relative to the pool of saturated water at near-critical conditions of 373° C, 219 bar ($T_c = 374\ 15°C$, $P_c = 221\ 29$ bar). The model assumes that location of the bubbles are spaced on a solid surface in a square pattern separated by the Taylor fastest-growing wavelength given by Berenson [2]

$$\lambda_o = 2\,\pi\sqrt{\frac{3\sigma}{(\rho_l - \rho_g)\,g}} \tag{1 1}$$

The bubble diameter and the bubble height in Berenson's model are considered to be proportional to the bubble spacing. However, the characteristic length in the present investigation, for presenting the pertinent dimensionless parameters, such as, Nusselt number has been considered as

$$\lambda = \sqrt{\frac{\sigma}{(\rho_l - \rho_g)\,g}} \tag{1 2}$$

1.2 Scope of the Present Work

In this investigation we explore by the numerical simulations discussed in the subsequent chapters, the nature of the heat transfer processes and particularly the influence of the large variations in the thermal and transport properties of the vapor

The present study has significant applications in order to understand thermal issues in high speed civil transport, heat treatment of metals, nuclear reactor design, cryogenics, cooling for superconducting applications and many other thermal storage systems

1.3 Layout of the Thesis

In chapter-1, we have already discussed the genesis of the problem Chapter-2 provides a review of the literature in the boiling flows In this chapter, different methods for simulating free surface flows and the evaluation of volume of fluid methods (VOF) have also been discussed The mathematical formulation of the problem for simulation is presented in Chapter-3 This chapter contains the governing equations, boundary conditions, interface tracking algorthim, jump conditions at liquid vapor interface and numerical procedure Kernel function calculation for smoothing void field and LVIRA algorithm for defining interface location are also discussed here in detail Chapter-4 present results for the current simulation Here the nature of periodic bubble release pattern, distribution of wall heat flux at various time instant, temperature contours and velocity vectors are shown and discussed The comparison of computed space averaged Nusselt number value with different correlations is also done in this chapter. Chapter-5 includes the concluding remarks and the scope for the further research

Chapter 2

Review of Literature

2.1 Review of Boiling Flows

Numerous publications in the open literature document that there has been a long–lasting interest among the researchers to clarify interface transport mechanisms in liquid–vapor phase change processes In the past, appropriate studies in this field were carried out experimentally Albeit having very useful contributions in the development of the subject, the early investigations could not provide the physical details needed for a closer understanding of the bubble formation and the time varying heat transfer characteristics Experimental studies in boiling have yielded several empirical correlations that are valid for specific cases Only the advancement of computational techniques have opened up new ways to carry out the investigations in detail on boiling, revealing the nuances of the interface transport processes. The volume of fluid (VOF) method of Hirt and Nichols [9] forms the building block of computations involving two fluids separated by a sharp interface The VOF method has been modified very successfully by Welch and Wilson [30] to simulate horizontal film boiling Son and Dhir [22] have also performed complete numerical simulation of the evolution of the vapor-liquid interface during film boiling on a horizontal surface. In another approach, Son and Dhir [23] have modified the level set method of Sussman et al [24] to perform numerical simulation of film boiling At low wall superheats, they have observed the upward movement of the interface initiating the vapor bubble formation Having released the bubble, the interface drops down alternatively at

the nodes and anti-nodes of a Taylor wave

Juric and Tryggvason [11] have performed excellent simulations of film boiling using single field formulation where one set of conservation equations are written for the entire flow field and different phases are treated as one fluid with variable material properties They have used source terms in the continuity and the energy equations as an enhancement of the method of Unverdi and Tryggvason [25] Interfacial source terms for surface tension, interface mass transfer and latent heat are added as delta functions that are non-zero at the interface boundary Banerjee and Dhir [1] have performed direct simulation of evolving interface during sub-cooled film boiling The simulation provides the shape and growth rates of the interface and the associated thermal behavior

The overview on numerical simulations of pool boiling has been authoritatively reviewed by Dhir [7] He pointed out that numerical simulations of evolving liquid-vapor interfaces during a phase change process such as boiling provide significant additional insights into the phenomena More recently Welch and Rachidi [28] developed another VOF based interface tracking method to explore film boiling on a horizontal surface and considered a conjugate problem between a solid wall and the boiling fluid They carried out the analysis considering constant thermal properties at the saturation temperature, whereas it has been seen from the NBS (National Bureau of Standards /NRC (National Research Council of Canada) Table (Table 4 1) that at near critical pressure, the transportive thermal properties of vapor vary significantly with temperature The present work is an extension of the work by Welch and Rachidi [28] with respect to the variable thermal properties

2.2 Overview of Methods for Simulation of Free Surface Flows

Fluid flows with free surfaces or material interfaces occur in a large number of natural and technological processes Free surfaces mean here to be the surfaces on which discontinuities exist in one or more variables Often properties that depend on the shape of the interface itself (e g , surface tension) play an important role in the dynamics of

the problem, and the physics (e g , capillarity) can drive the flow making it essential to accurately determine the position, curvature, and topology of the interface

All numerical simulations of free surface flows require a discretisation or nodalization to allow numerical treatment on computers There are two fundamentally different approaches Eulerian methods use a frame of reference (discretisation grid or mesh, control volumes, nodes, etc) fixed in space, and matter (fluids) moving through this frame of reference Lagrangian methods instead use a frame of reference (marker particals, grid or mesh, etc) fixed to and moving with the matter Lagrangian method is less useful if strong distortions of the flow occur, or if the topology changes, for example, as moving boundaries merge or break up Then, the frame of reference has to be re-initialized (re-meshing, re-ordering of points, etc), which may be very cumbersome Eulerian methods, on the other hand, tend to be less accurate due to numerical diffusion

For our problem, we expected strong distortions, and many topology changes during detachment or break-up of bubble We therefore chose an Eulerian method, in spite of its lower accuracy

The first method capable of modeling gas-liquid flow, separated by a moving interface, was the Marker and Cell method (MAC) of Harlow and Welch [8] This was in fact a combination of an Eulerian solution of the basic flow field, with Lagrangian marker particles attached to the liquid to distinguish it from the gas While the staggered mesh layout and other features of MAC have become a model for many other Eulerian coades, the marker particles proved to be computationally too expensive and have been rarely used.

Subsequent to MAC, Volume of Fluid (VOF) method of Hirt and Nichols [9] became popular Instead of marker particles, a liquid volume-fraction field, usually named α is used It indicates for each computational cell its liquid fraction ($\alpha = 1$ liquid, $\alpha = 0$ gas, and $0 < \alpha < 1$ for an interfacial cell). α is a property of the fluid with which it moves The key feature of a VOF method lies in its technique for advecting α standard finite-difference methods suffer from numerical diffusion, which smoothen α excessively Therefore, special, often geometry-based, methods are used to advect α

The α field is the only phase information stored in VOF methods Approximate interface locations are found from a so-called interface reconstruction This is needed for advecting α, for determining the local properties (density, viscosity) and for better graphical representation In earlier versions, usually called SLIC (Simple Line Interface Method)

after Noh and Woodward [15], the interface is approximated as piecewise constant, where interface within each cell are assumed to be the lines aligned with one of the logical mesh coordinates

More accurate reconstructions are possible with PLIC (Piecewise Linear Interface Construction) methods, pioneered by Youngs [31] Youngs' method positioned each reconstructed interface line, defined by a slope and intercept, within the control volume cell The slope of the line is given by the interface normal (gradient of the volume fractions), and the intercept follows from invoking the volume conservation Many extensions and enhancements to the significant work of Youngs have occurred since its introduction Recently, modification of Youngs method has been done with the help of Least Squares Volume of Fluid Interface Reconstruction algorithm (LVIRA) method of Puckett et al [17] This method is well implemented by Welch and Rachidi [28] for exploring film boiling on a horizontal heated surface. This method has several advantages the fluxes of α , with which the phase field α is updated, can be determined more accurately, and essentially free of numerical diffusion The interface area is known approximately, so that surface tension and mass transfer can be applied more easily Fluid properties (density and viscosity) can be allocated accurately Finally, the straight lines also give a graphical representation of good quality

Most earlier versions of PLIC used rectangular, regular grids, and were in two dimensions only Kothe et al. [13] and Welch et al. [29] showed that PLIC-VOF can be extended to general, hexahedral meshes in three dimensions without additional difficulty

The Level Set Method of Osher and Sethian [16] is another useful method for interface tracking and reconstruction For interface tracking, they use a new field variable ϕ (a smooth function), the absolute value of which indicates the shortest distance to the interface, but is positive in one fluid and negative in the other The interface is at the set of points where $\phi = 0$

Much the same as α in the VOF method, ϕ is approximated as a property of the fluid with which it moves, and thus follows a simple advection equation $D\phi/Dt = 0$ However, due to flow distortions, ϕ deviates more and more from the true distance to the interface, and therefore has to be re-initialized every couple of time-steps by the solution of a differential equation. For numerical reasons, properties such as density or viscosity cannot change sharply at the interface, but require a smooth transition (usually fitted with a sine function) of about three to five meshes wide Although, ϕ can be discretely conserved, the mass enclosed by the zero level set of ϕ is not conserved However, Chang et al [5]

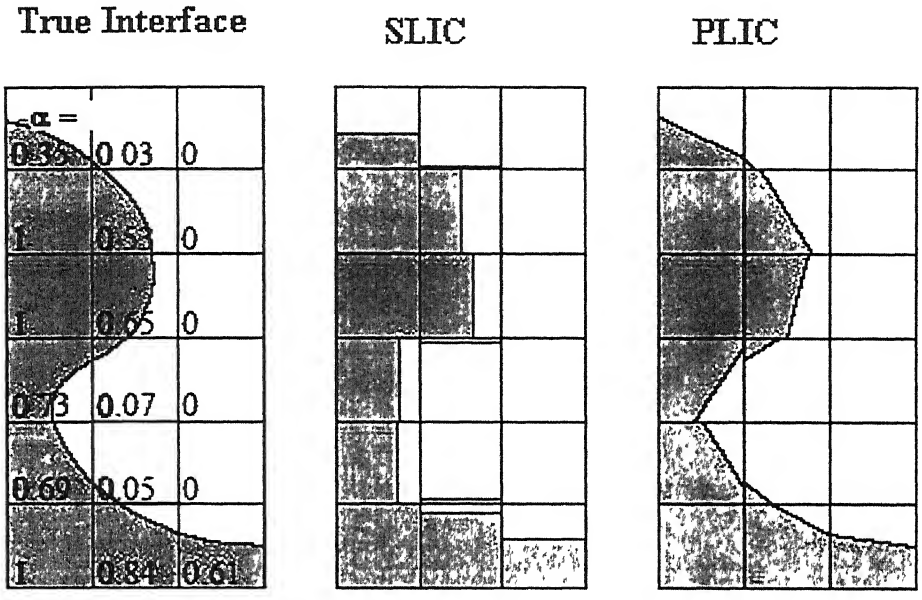

Figure 2 1 A true interface, and the corresponding void field. Reconstruction of the interface by horizontal or vertical lines (SLIC) and by straight lines of arbitrary inclination (PLIC)

that this can be overcome

2.3 Epilogue

The Volume of Fluid (VOF) and the Level Set Method are the two attractive methods for handling flows with interface and free surface However, we preferred to use a variant of Volume of Fluid method The method followed here is computationally simple for its explicit way of advancing the liquid-vapor interface Furthermore, the method includes a very elegant version of a Continuum Surface Tension (CST) model of Brackbill et al , [3] The CST model will be discussed in a subsequent chapter The numerical technique in this investigation also uses a modified version of LVIRA method due to Welch and Rachidi [28]

Chapter 3

Formulation of the Problem

3.1 Governing Equations

The mass, momentum and energy conservation equations for the incompressible Newtonian fluids for the liquid and vapor phases are given by

$$\frac{\partial U_i}{\partial x_i} = 0 \tag{3.1}$$

$$\rho \left(\frac{\partial U_j}{\partial t} + \frac{\partial U_i U_j}{\partial x_i} \right) = - \frac{\partial p}{\partial x_j} + \frac{\partial}{\partial x_i} \left(\mu \frac{\partial U_j}{\partial x_i} \right) \tag{3.2}$$

$$\left(\frac{\partial \ (\rho \ c_p \theta)}{\partial t} + \frac{\partial (\rho \ c_p \theta \ U_j)}{\partial x_j} \right) = \frac{\partial}{\partial x_j} \left(k \ \frac{\partial \ \theta}{\partial x_j} \right) \tag{3.3}$$

Here, U_j, p, c_p, ρ, θ, μ and k are the fluid velocity, pressure, specific heat, density, temperature, viscosity and thermal conductivity, respectively The dissipation term in the energy equation has been neglected

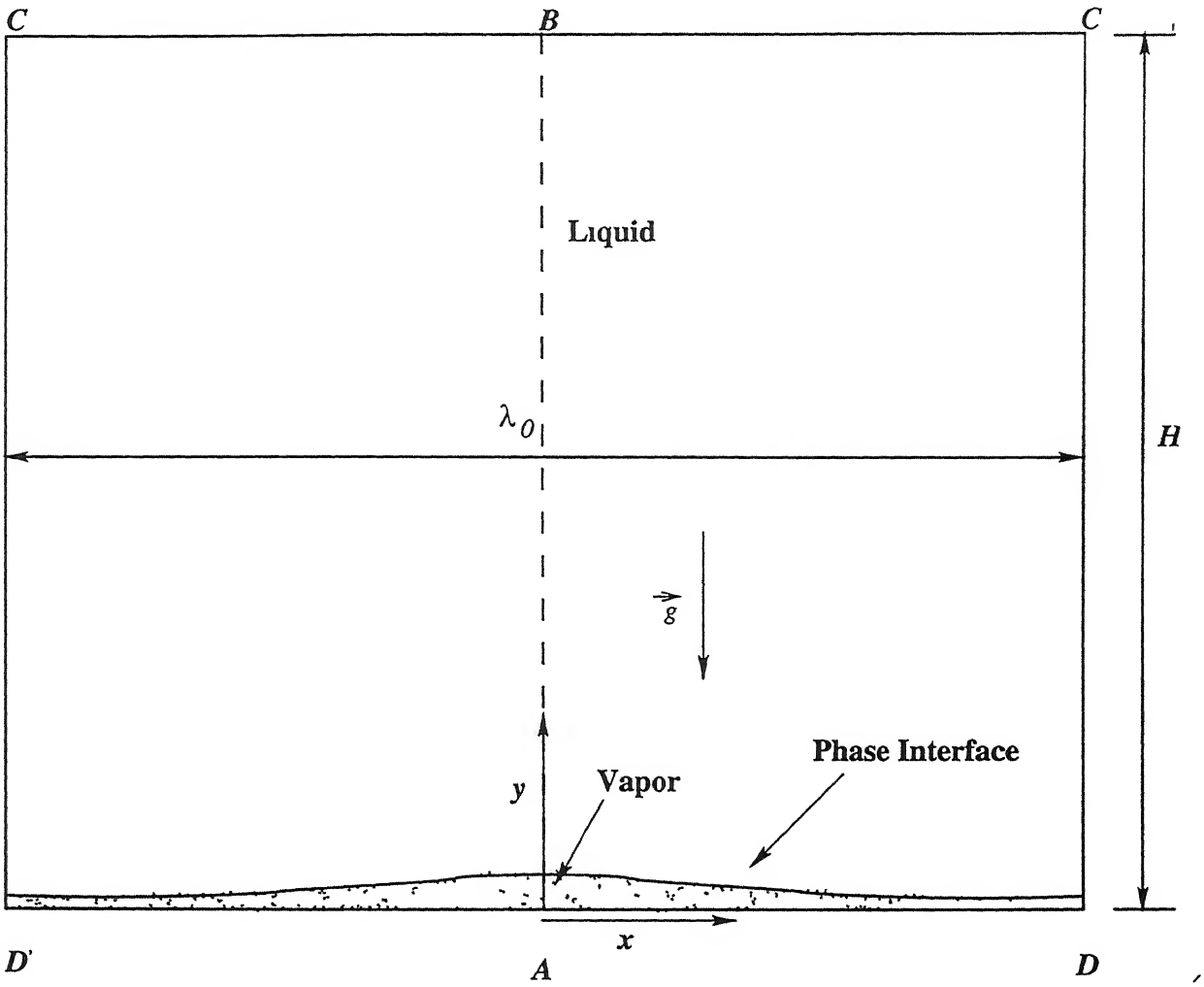

Figure 3 1 The domain for the simulation of film boiling

3.2 Boundary Conditions

Figure 3 1 shows the domain of interest for the present investigation The simulation is planar, two-dimensional The computational domain is given by ABCD The boundary conditions are symmetry conditions at the left and right boundaries

$$\text{at } x = 0 \text{ and } x = \lambda_o/2 \qquad u = 0, \ \frac{\partial v}{\partial x} = 0, \ \frac{\partial \theta}{\partial x} = 0$$

Constant wall temperature condition is used on the solid-fluid interface

$$\text{at } y = 0 \qquad \theta = \theta_{sup}$$

Outflow boundary conditions are used on the top surface of the domain

$$\text{at } y = H \qquad \frac{\partial u}{\partial y} = \frac{\partial v}{\partial y} = \frac{\partial \theta}{\partial y} = 0, P = P_o$$

The outlet pressure is the saturation pressure less the hydrostatic pressure difference from the initial film level to the outlet The boundary condition at the vapor liquid interface is of special concern in this study In order to address this issue, a suitable interface tracking method has been implemented

3.3 Interface Tracking

The presence of two phases in the fluid requires handling of the phase interface We advect the interface using enhancement of VOF method of Hirt and Nichols [9] due to Youngs [31] The method of Youngs is implemented at the end of a time cycle to calculate the new density field using conservation of mass for each cell

$$\frac{\partial}{\partial t}\int_{V_c} \rho dV + \int_{S_c} \rho \mathbf{v} \cdot \mathbf{n} dS = 0 \tag{3 4}$$

where V_c is the cell volume and S_c is the cell surface The symbol v is used for the fluid velocity Once, the new cell densities are found, the cell void fractions are calculated using

$$\alpha = \frac{\rho - \rho_g}{\rho_l - \rho_g} \tag{3 5}$$

Here ρ_l and ρ_g are the densities of the saturated liquid and saturated vapor, respectively The implementation of the method of Youngs has been well documented in Rider and Kothe [20], Rudman [21] and Welch and Wilson [30] The phase interface is represented by piecewise linear curves Figure 3 2 shows a typical two phase cell The orientation of the curve within each two phase cell is determined using the procedure based on LVIRA method of Puckett et al [17]

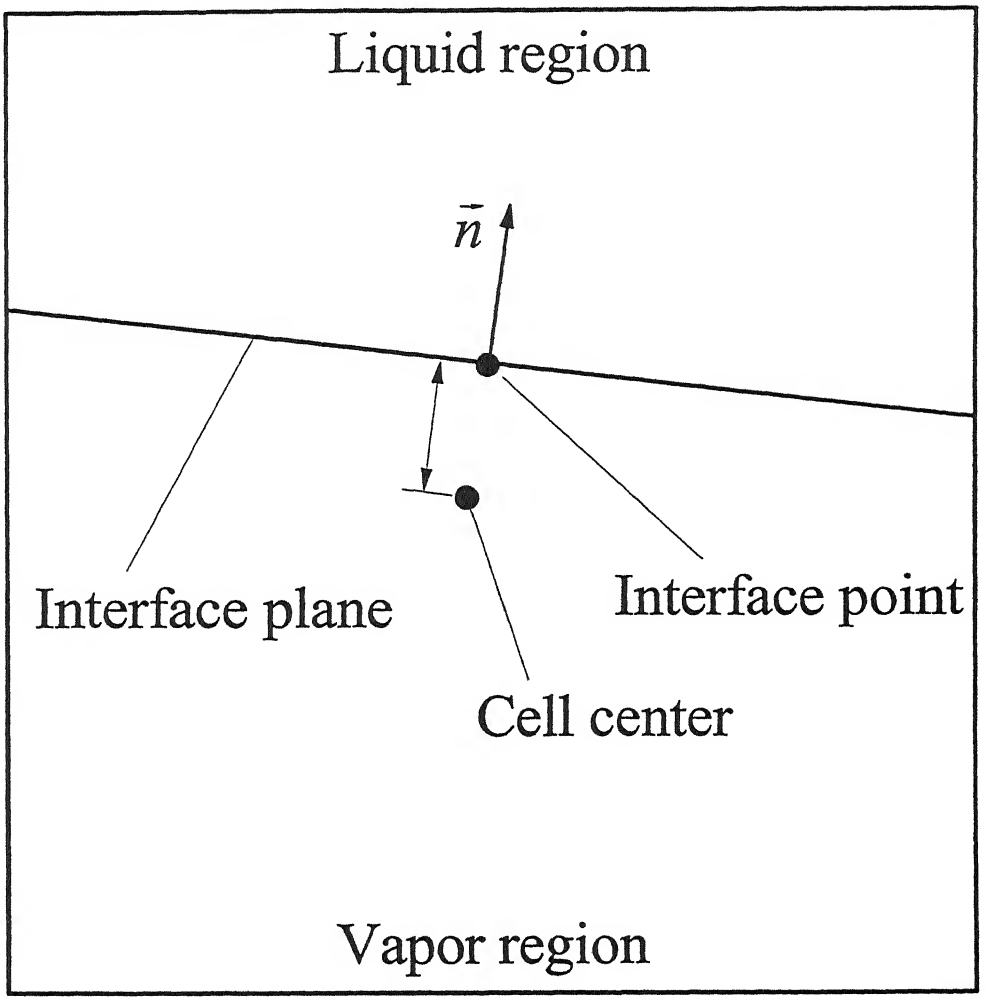

Figure 3 2 A typical two phase cell with piecewise linear interface

3.3.1 Least Squares Interface Reconstruction Algorithm (LVIRA)

Least Squares Interface Reconstruction Algorithm (LVIRA) is a volume-of-fluid *interface reconstruction algorithm* for constructing an approximation to the interface at the beginning of every time cycle, given the values of the void fraction $\alpha_{i,j}$ This algorithm produces a linear approximation to the interface which are also continuous across the cell boundaries, in each two phase cell The interface is uniquely defined by the unit normal, $\mathbf{n}$, the orientation of the interface and the offset distance, l Therefore, LVIRA can be understood as a function which returns $\mathbf{n}, l$, given the void fraction of each two-phase cell

In the LVIRA the approximate interface in a two phase cell (i, j) is determined by minimization of the following function in the 3 × 3 block of cells centered on the (i, j) cell

$$G_{i,j}(\mathbf{n}) = \sum_{k,l=-1}^{1} \{\alpha_{i+k,j+l} - \hat{\alpha}(\mathbf{n}, l)_{i+k,j+l}\}^2 \tag{3 6}$$

subject to the constraint at the center cell of the three by three block of cells

$$\alpha_{i,j} = \hat{\alpha}\ (\mathbf{n}, l)_{i,j} \tag{3.7}$$

Here $\alpha_{i,j}$ is the actual void fraction of the cell (i, j) and $\hat{\alpha}(\mathbf{n}, l)_{i,j}$ is the function that maps the line with orientation $\mathbf{n}$ and offset length l into a void fraction of the cell (i,j) The offset length, l, is obtained by satisfying the constraint The function $G_{i,j}$ $(\mathbf{n})$ is the squared deviation of the actual void fraction from the void fraction given by the mapping using the same line for the entire three by three block of cells centered at cell (i,j). Minimization of this function rotates and translates the line in such a way as to ensure that the mapping is exact for the center cell and that the straight line associated with this mapping is the best fit to the void field for the neighboring cells. The result of the minimization is the calculation of the unit normal and the offset length $(\mathbf{n}, l)$ for the cell at the center of the three by three block This calculation is performed for all the mixture cells, satisfying the constraints that the mapping $\hat{\alpha}(\mathbf{n}, l)_{i,j}$ returns the actual void fraction This constr ained minimization of the function $G_{i,j}(\mathbf{n})$ is a nonlinear problem requiring an initial estimate for $\mathbf{n}$ This initial $\mathbf{n}$ is the value determined by the modified VOF method of Youngs [31] as

$$\mathbf{n} = \frac{\nabla\alpha}{|\nabla\alpha|} \tag{3 8}$$

We note that this algorithm is second order method and has the property that it reproduces linear interfaces exactly

3.3.2 Direction Split Approach

Given the orientation of the planar surface that represents the interface in a cell, we determine the location of the oriented surface, such that the surface partitions the cell

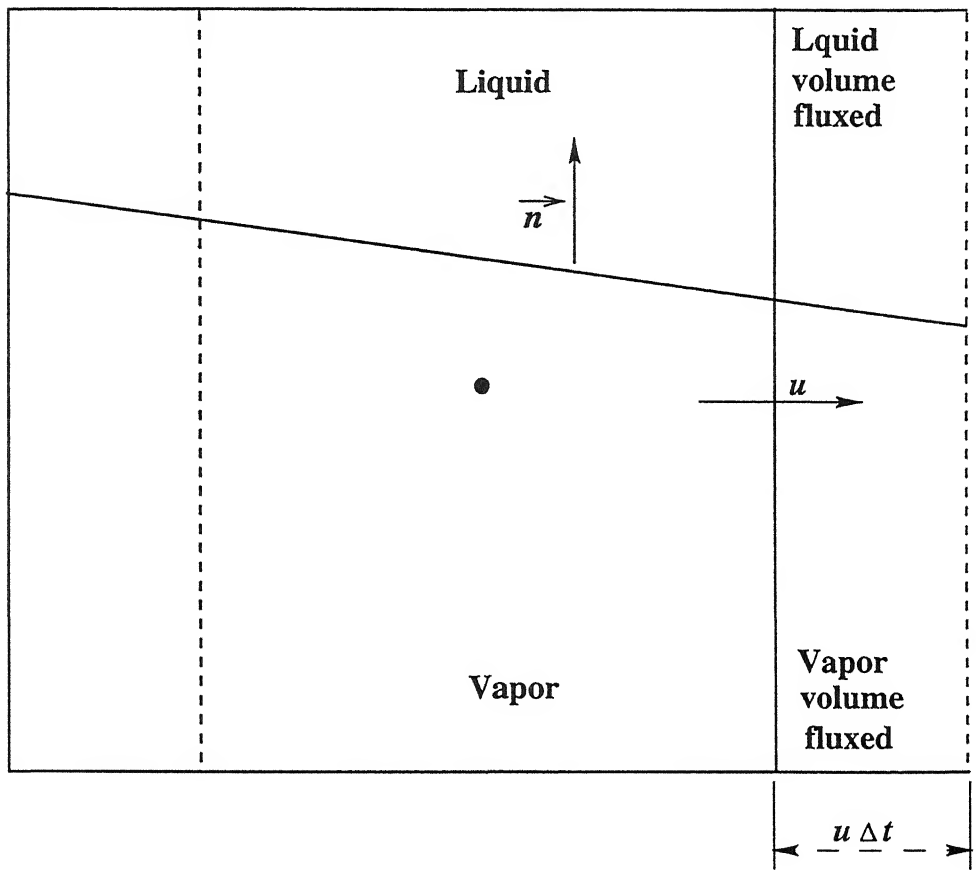

Figure 3 3 Schematic of cell flux calculation

into liquid and gas regions of correct volume, based upon the void fraction (which is defined as the volume fraction of the liquid) of the cell Given the location of the planar interface (i e , knowing $\mathbf{n}$, l) in each two phase cell and the velocity at a junction face between two cells, the mass flux is determined from simple volumetric considerations Once the mass is fluxed across the cell boundaries in one direction (Fig 3 3), the interface is reconstructed before mass is fluxed in the second direction This is the Direction Split Approach of Rudman [21]

3.4 Jump Conditions at Liquid Vapor Interface

The mass transfer across the interface is modeled following Welch and Rachidi [28] We consider a computational cell containing a volume of the liquid phase adjacent to a volume of the vapor phase We write a mass balance for each phase as

$$\frac{d}{dt}\int_{V_g(t)} \rho dV + \int_{S_g(t)} \rho \mathbf{v}\ \mathbf{n} dS + \int_{S_I(t)} \rho(\mathbf{v}-\mathbf{v}_I)\ \mathbf{n} dS = 0 \tag{3 9}$$

$$\frac{d}{dt}\int_{V_l(t)} \rho dV + \int_{S_l(t)} \rho \mathbf{v}\ \mathbf{n} dS + \int_{S_I(t)} \rho(\mathbf{v}-\mathbf{v}_I)\ \mathbf{n} dS = 0 \tag{3 10}$$

Here, V_l, S_l, V_g, S_g are the volume and surface of the liquid and vapor regions, respectively S_I is the phase interface at the common boundary of the two regions, moving with velocity $\mathbf{v}_I$ The normal vector $\mathbf{n}$ points into the liquid phase on S_I From the above, and taking into account the incompressibility of each phase, and under the situation that the overall volume is time invariant, the conservation of mass statement for the cell volume is determined

$$\int_{S_c} \mathbf{v}\ \mathbf{n} dS + \int_{S_I(t)} \|(\mathbf{v}-\mathbf{v}_I)\|\ \mathbf{n} dS = 0 \tag{3 11}$$

Here, $\|.\|$ indicates the jump in the variable of interest across the phase interface and S_c is the surface bounding the computational cell The mass and energy jump conditions at the interface may be estimated as

$$\|\rho(\mathbf{v}-\mathbf{v}_I)\|\ \ \mathbf{n} = 0 \tag{3 12}$$

$$\|\rho h(\mathbf{v} - \mathbf{v}_I)\| \cdot \mathbf{n} = -\|\mathbf{q}\| \, \mathbf{n} \tag{3 13}$$

entails the contribution of jump in the conservation of mass equation as

$$\|(\mathbf{v} - \mathbf{vI})\| \;\; \mathbf{n} = (\frac{1}{\rho_l} - \frac{1}{\rho_g}) \frac{\|\mathbf{q}\| \, \mathbf{n}}{h_{lg}} \tag{3 14}$$

Here, h is the enthalpy and $h_{lg} = h_g - h_l$ is the latent heat of vaporization while $\mathbf{q}$ is the heat flux vector We assume the phase interface to be at the saturation temperature of the liquid pressure

$$\theta_I = \theta_{sat}(P_l) \tag{3 15}$$

The set of equations, Eq (3 13) through Eq (3 15), incorporates various simplifying assumptions Surface properties other than surface tension are neglected We neglect kinetic energy and viscous work terms as well as surface tension work terms in the energy jump and we have also neglected the viscous dissipation in the energy equation These are common approximations in the analysis of liquid-vapor phase change phenomena [4] and have been used in the numerical studies of liquid-vapor phase change [22, 23, 27] The temperature condition given by Eq (3 15) is a common approximation for which justification may be found in [23]

The energy jump condition includes the effect of heat flux vector (normal to the interface) on the mass transfer rate across the interface The heat flux vector will generally be discontinuous and any smoothing of this vector will distort the mass transfer amount We utilize the interface geometry associated with the VOF method to construct a proper heat flux jump source term for use in Eq (3 14) By a proper heat flux jump, we mean that the normal components of the temperature gradients are calculated without reaching across the phase interface The required geometry is provided in the advection step described above and is shown in Fig 3 3 Given the unit normal vector, $\mathbf{n}$ and the parameter l which provides the location of the interface we apply the temperature condition, Eq. (3 15), to the point located at the center of the piecewise linear segment (the interface point in Fig 3 2) It is then a simple matter to calculate liquid side temperature gradients as well as vapor side temperature gradients We then are able to construct a proper heat flux jump across the phase interface by multiplying the normal temperature gradients in each phase by their corresponding conductivities In addition, it is important that the cells proximal to the interface but not containing the phase interface see proper temperature gradients in the convection and diffusion terms of the energy equations We ensure this by using the

temperature gradients used in forming the energy jump condition to extrapolate liquid and vapor temperatures at mixture cell centers thus ensuring that the cells neighboring mixture cells also see the proper temperature gradients

3.5 Modified Momentum Equation

The momentum equations are augmented using the continuum surface tension model of Brackbill et al [3] in the following way

$$\rho(\tilde{\alpha})(\frac{\partial \mathbf{v}}{\partial t} + \mathbf{v}\ \nabla\mathbf{v}) = -\nabla P + \rho(\tilde{\alpha})\mathbf{g} + \nabla\ \ [\mu(\tilde{\alpha})(\nabla\mathbf{v} + (\nabla\mathbf{v})^T)] + \sigma\kappa\nabla\tilde{\alpha} \qquad (3\ 16)$$

where $\tilde{\alpha}$ is a smoothened void field and κ is the curvature of the surface defined by smoothened void field The surface tension force is applied to a transition region of nine cells thick centered at the interface The density and viscosity vary with the void fields as

$$\rho(\tilde{\alpha}) = \tilde{\alpha}\rho_l + (1 - \tilde{\alpha})\rho_g \qquad (3\ 17)$$

$$\mu(\tilde{\alpha}) = \tilde{\alpha}\mu_l + (1 - \tilde{\alpha})\mu_g \qquad (3\ 18)$$

In the sequel, it can be said that for the interface cells, we use the augmented momentum Eq (3 16), the modified conservation of mass Eq. (3 11) and the energy jump condition given by Eq. (3 13). The discontinuity of the velocity field, the velocity gradients, and the viscosity are treated by smoothing

3.6 Smoothing of the Void Field

The basic idea of all continuum surface tension (CST) models is the representation of surface tension as a continuous force per unit volume that acts in a neighborhood of the interface The non smoothed void field changes abruptly across the interface While calculating the surface tension force, applicable to a transitional region, first and second

order spatial derivatives of α are required These derivatives causes problem with CST formulation, if they are not smoothed out

Here we calculate a smooth void field by convolving a discrete form of void fraction with a smooth kernel (a eighth-degree polynomial) This convolution results in a smooth void field, denoted by $\tilde{\alpha}$, given by,

$$\tilde{\alpha}(x) = \int_{\Omega_k} \alpha(x)\Gamma(x - x')dS \tag{3 19}$$

where $\Gamma(x)$ is the kernel function and Ω_k is defined by a parameter ϵ that essentially controls the smoothed interfacial thickness

The choice of kernel is critical for the design of an accurate CST model The basic requirements for selecting a kernel function are as the following,
(i) have compact support,
(ii) monotonically decreasing,
(iii) be radially-symmetric,
(iv) be sufficiently smooth, i e , for some $k \geq 3$, kernel should be k times continuously differentiable,
(v) have a normality property, i e , $\int_{\Omega_k} \Gamma(x, \epsilon) = 1$,
(vi) approach the Dirac delta function $\delta(x)$ in the limit $|\Omega_k| \longrightarrow 0$

In the present work we used a eighth degree polynomial kernel, denoted Γ, given by

$$\Gamma(x^{'} - x) = \begin{cases} \left[1 - \left(\frac{|x-x^{'}|}{\epsilon}\right)^2\right]^4 & |x - x^{'}| < \epsilon \\ 0 & |x - x^{'}| \geq \epsilon \end{cases} \tag{3 20}$$

where A_c is a normalization constant that ensures $\int_{\Omega_k} \Gamma(x, \epsilon) = 1$ The kernel $\Gamma(x, \epsilon)$ satisfies all the six properties listed above We have used $\epsilon = 4\delta x$, where δx is the grid spacing The curvature, κ, is calculated using the smoothed void field as,

$$\kappa = -\nabla \hat{\mathbf{n}} \tag{3 21}$$

where,

$$\hat{\mathbf{n}} = \frac{\nabla\tilde{\alpha}}{|\nabla\tilde{\alpha}|} \tag{3 22}$$

3.7 Numerical Procedure

The spatial discretization of governing equations is obtained using a staggered grid arrangement of Harlow and Welch [8] with scalars located at the cell centers and velocity components located at the center of the cell faces The convection terms of the momentum equation are discretized by higher order methods using an ENO discretization scheme (see Chang et al [5]) The convection terms in energy equation are discretized by QUICK [14] The temporal discretization is described by a semi-implicit forward Euler method We begin a time cycle by solving the explicit energy equation in the bulk fluid phases

$$\theta^{n+1} = \theta^n + \frac{\delta t}{\rho c_p}[-\mathbf{v}\,\nabla(\rho c_p\theta) + \nabla(k\nabla\theta)]^n \tag{3 23}$$

After every time step with the help of new temperature field, thermal conductivity and specific heat at each cells are calculated The thermal properties and temperature field thus obtained are used to form the interfacial heat flux jump appearing in the mass source term The continuity and momentum equations are discretized in time as

$$\int_{S_c} \mathbf{v}^{n+1}\,\mathbf{n}dS + \int_{S_l(t)} (\frac{1}{\rho_l} - \frac{1}{\rho_g})\frac{\|\mathbf{q}^{n+1}\|\,\mathbf{n}}{h_{lg}}dS = 0 \tag{3 24}$$

$$\mathbf{v}^{n+1} \doteq \mathbf{v}^n - \delta t(\mathbf{v}\,\nabla\mathbf{v})^n - \frac{\delta t}{\rho^n}\{\nabla P^{n+1} + (\rho\mathbf{g})^n + \nabla\,[\mu(\nabla\mathbf{v} + (\nabla\mathbf{v})^T)]^n + \sigma(\kappa\nabla\tilde{\alpha})^n\} \tag{3 25}$$

The velocity for the new time step is eliminated from these discrete equations and resulting pressure equation is solved by an iterative method based on a preconditioned conjugate gradient scheme of Van der Vorst [26] that has been implemented by Welch and Rachidi [28] Once the pressure at the new time level is obtained, the velocity at the new time level is found from the discrete momentum equations and the new density field is found from Eq (3 4) as

$$\rho^{n+1} = \rho^n + \delta t \int_{S_c} \rho\mathbf{v}^{n+1}\,\mathbf{n}dS \tag{3 26}$$

As discussed earlier, at this stage LVIRA algorithm is invoked The cells that are not mixture cells, or are not adjacent to mixture cells, do not require this treatment Once the new density field is found, the new void fraction may be calculated and the mixture cell interfacial geometry can be updated

The numerical scheme is based on the explicit time-advancement strategy The time step is determined from the limit imposed on a capillary wave traveling in an infinite medium [30] The wave is not allowed to travel more than half a cell width during a time step

Chapter 4

Results and Discussion

The simulations were performed with variable and constant thermal properties of the fluid The variable properties are indicated in Table 4 1 The constant properties are evaluated at near-critical conditions of 373° C and 219 bar These properties are given in Table 4 2 The computational domain chosen for the present simulation is shown in Fig 3 1 Since the problem is symmetric, a computational domain with width $\lambda_o/2$ was chosen In the present simulation the numerical values of λ_o and λ are 2 270 mm and 0 2087 mm, respectively The height of the domain, H was set as λ_o with initial interface height, δ set to

$$\delta = \frac{\lambda_o}{128}\left\{2 + \cos\left(\frac{2\pi x}{\lambda_o}\right)\right\} \tag{4 1}$$

We first present results of a convergence study undertaken to find an adequate grid resolution For this, simulations were performed with three grid-meshes, viz , 90×180, 180×360 and 360×720 Figure 4 1 shows the interfacial shape at the instant of bubble release from the surface for the above-mentioned grid resolutions We observe that the 180×360 and 360×720 produce nearly identical results, hence, we choose the 180×360 grid for our subsequent simulations The same simulation run on 180×360 with the time step halved also gives nearly identical results as seen in Fig 4 2 Thus the 180×360 grid with the time step used in spatial convergence study provides results converged in time and in space, and it is used for all the subsequent simulations

In the present simulation we considered water near the critical point and the vapor transportive thermal properties (thermal conductivity and specific heat of vapor) varying with

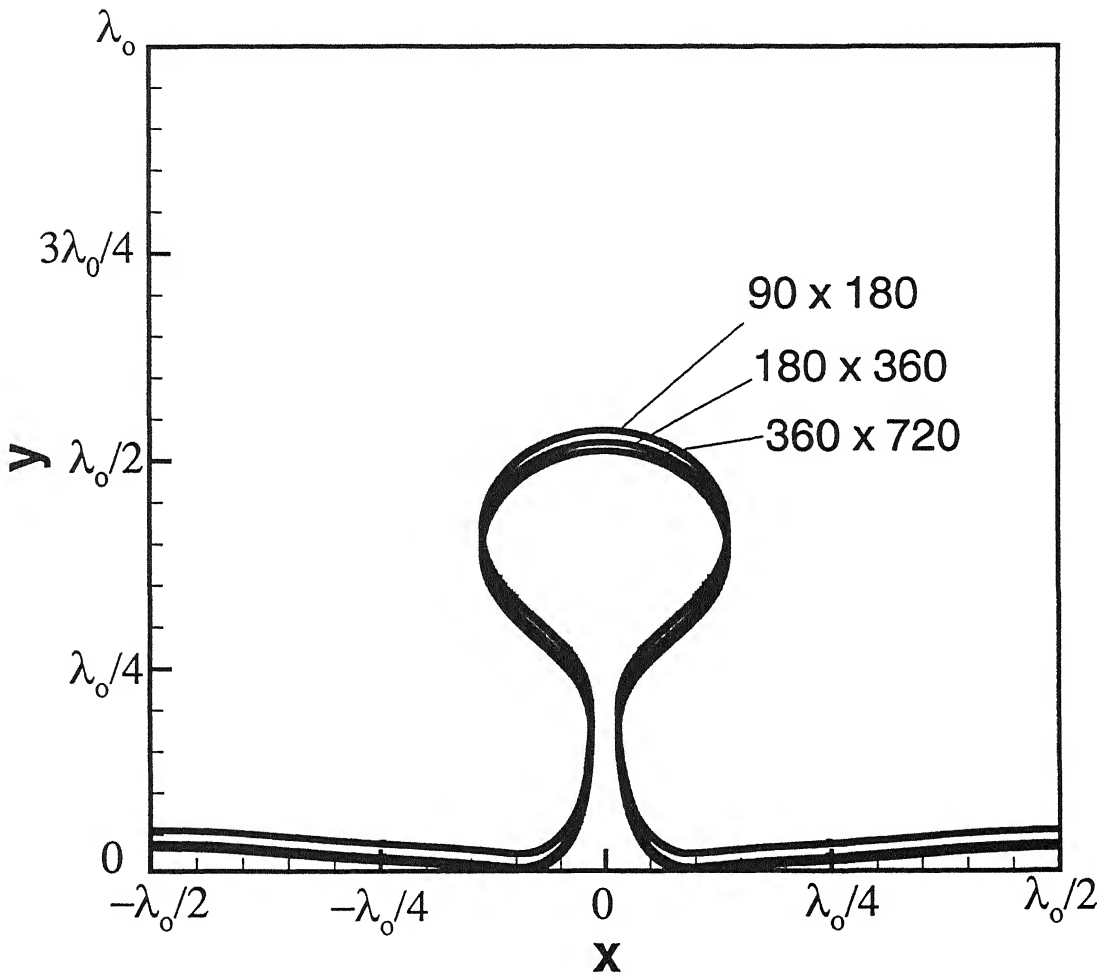

Figure 4 1 Bubble interface for three different grid resolutions

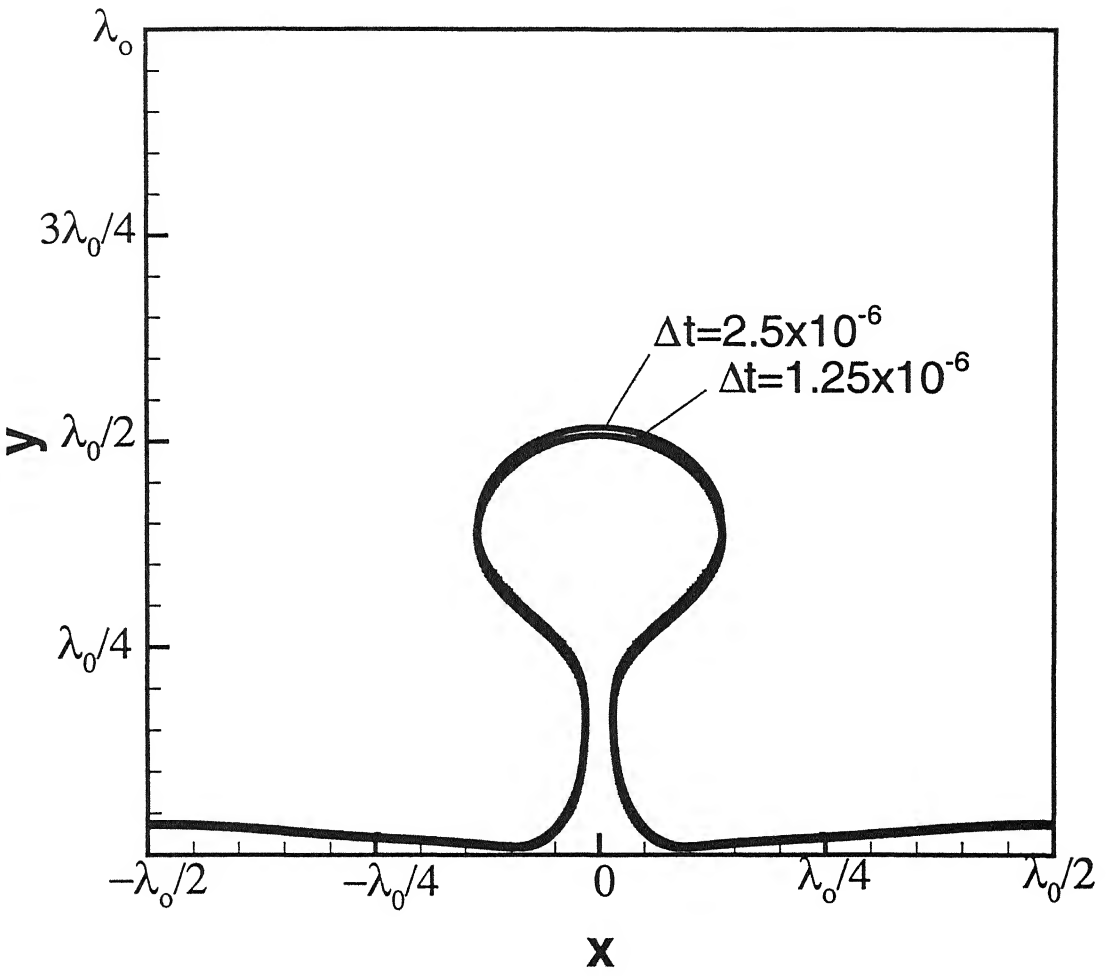

Figure 4 2 Bubble interface for two different time steps Grid resolution is kept as 180×360

temperature As mentioned earlier, the properties are given in Table 4 1 The interfacial properties and density are provided by Table 4 3 At the outset, we present numerical simulations showing growth of the bubble and its release pattern, with constant wall temperature boundary condition of 15°C superheat We used a data set of thermal properties (from Table 4 1) containing 10 values in the range of 15°C superheat and interpolated the properties to get intermediate values at any temperature corresponding to the cell temperature

$Temperature,^\circ K$	$k,\ W/mK$	$c_p,\ kJ/kgK$	$\mu,\ Pas$
646 15	0 5383	$3\ 520 \times 10^{2}$	$3\ 230 \times 10^{-5}$
647 81	0 2502	$0\ 4318 \times 10^{2}$	$2\ 912 \times 10^{-5}$
649 48	0 2126	$0\ 2854 \times 10^{2}$	$2\ 825 \times 10^{-5}$
651 15	0 1918	$0\ 2227 \times 10^{2}$	$2\ 775 \times 10^{-5}$
652 81	0 1777	$0\ 1864 \times 10^{2}$	$2\ 743 \times 10^{-5}$
654 48	0 1673	$0\ 1622 \times 10^{2}$	$2\ 720 \times 10^{-5}$
656 15	0 1591	$0\ 1448 \times 10^{2}$	$2\ 704 \times 10^{-5}$
657 82	0 1524	$0\ 1316 \times 10^{2}$	$2\ 692 \times 10^{-5}$
659 48	0 1468	$0\ 1211 \times 10^{2}$	$2\ 683 \times 10^{-5}$
661 15	0 1421	$0\ 1126 \times 10^{2}$	$2\ 676 \times 10^{-5}$

Table 4 1 Properties from NBS/NRC table for vapor phase.

Substance	$k,\ W/mK$	$c_p,\ kJ/kgK$	$\mu,\ Pas$
Liquid Water	0 5454	$2\ 18 \times 10^{2}$	$4\ 67 \times 10^{-5}$
Water Vapor	0 5383	$3\ 52 \times 10^{2}$	$3\ 23 \times 10^{-5}$

Table 4 2 Properties used for constant property simulation

$\sigma,\ N/m$	$h_{lg},\ kJ/kg$	$\theta_{sat},\ K$	$P_{sat},\ Pa$	$\rho,\ kg/m^3$ Liquid water	$\rho,\ kg/m^3$ Water vapor
$0\ 07 \times 10^{-3}$	276 4	646 15	$21\ 9 \times 10^{6}$	402 4	242 7

Table 4 3 Interfacial properties and density

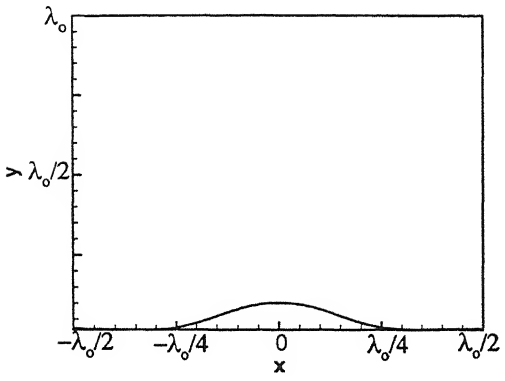
λo
y λo/2
−λo/2 −λo/4 0 λo/4 λo/2
x

(a)

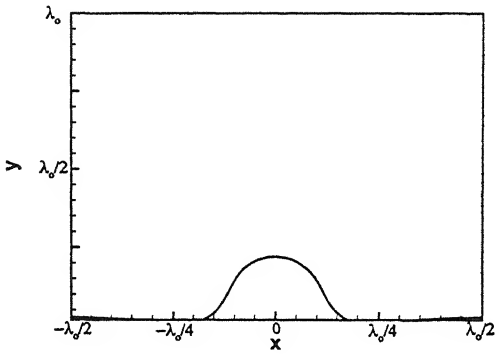
λo
y λo/2
−λo/2 −λo/4 0 λo/4 λo/2
x

(b)

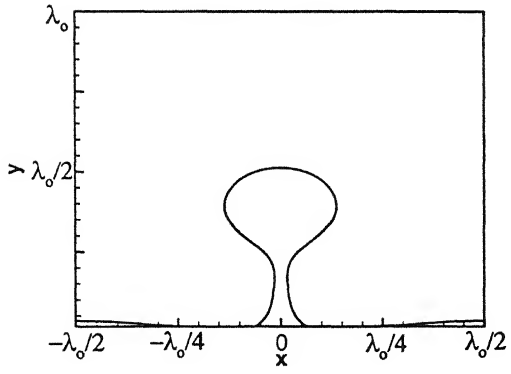
λo
y λo/2
−λo/2 −λo/4 0 λo/4 λo/2
x

(c)

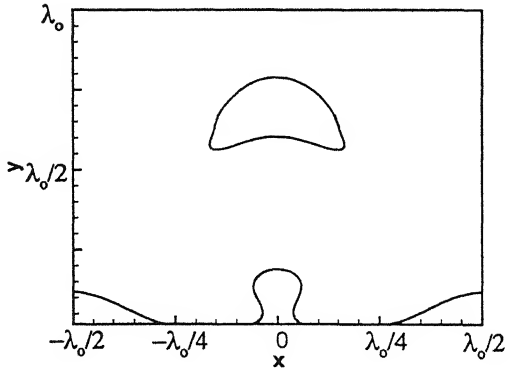
λo
y λo/2
−λo/2 −λo/4 0 λo/4 λo/2
x

(d)

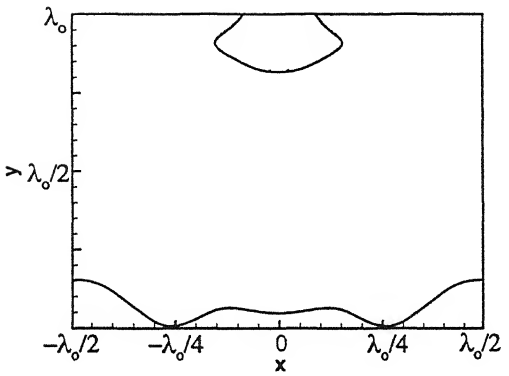
λo
y λo/2
−λo/2
−λo/4
0
λo/4
λo/2
x

(e)

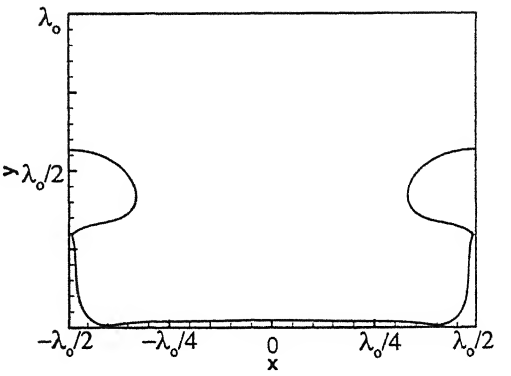
λo
y λo/2
−λo/2
−λo/4
0
λo/4
λo/2
x

(f)

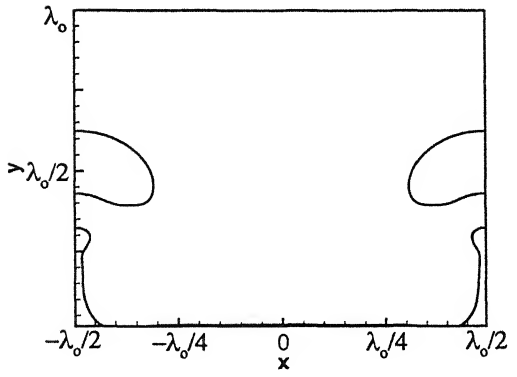
λo
y λo/2
−λo/2
−λo/4
0
λo/4
λo/2
x

(g)

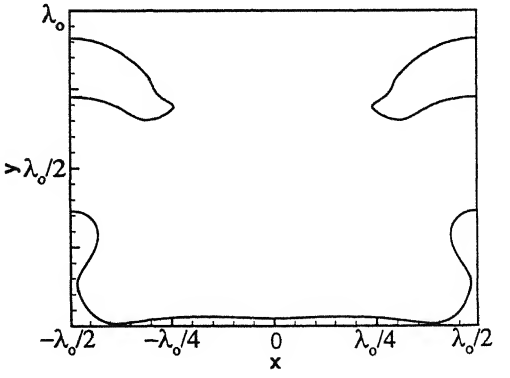
λo
y λo/2
−λo/2
−λo/4
0
λo/4
λo/2
x

(h)

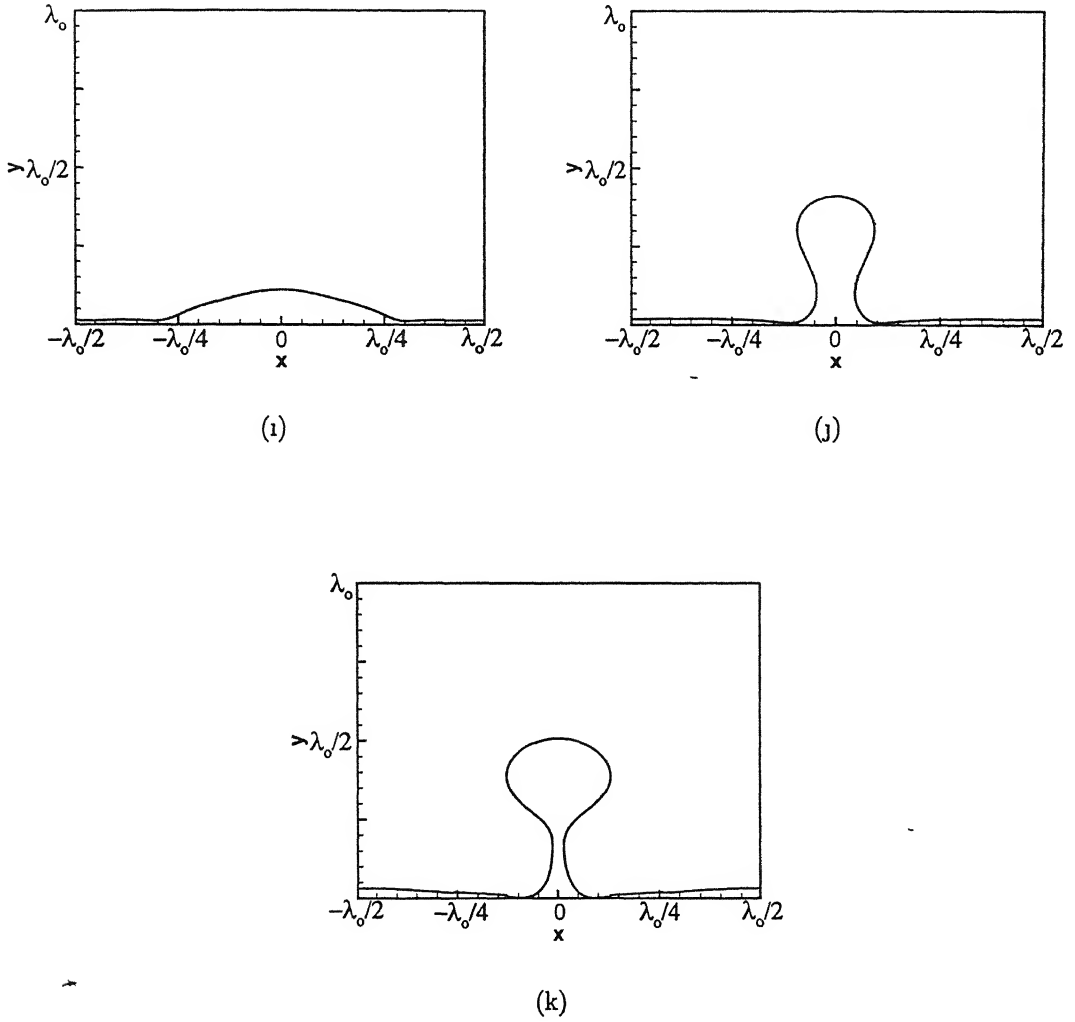

Figure 4 3 Bubble release from the constant wall temperature surface for two complete cycles

Figure 4 3 shows the periodic bubble release patterns with growing interface and varying vapor volume The steady cyclic growth and release of vapor bubbles is usually called ebullition cycle Starting with a thin vapor layer, gradually the bubble grows bigger Finally, the bubble reaches a limit at which it detaches The detached bubble moves upwards and leaves the domain of interest The released bubble leaves a very thin vapor film near the nodal position on the wall on which it had rested prior to its departure Due to the vapor production at the interface the thin vapor layer again grows in size The next bubbles tend to grow at the outer side walls, which are basically the anti-nodes according to the Taylor's wave length

The ebullition cycle or bubble release cycle is revealed through the sequence of varying interface boundary at different time instants. The mechanism for the repeating pattern can be described in the following way After the bubble is released from the surface, the vapor left behind experiences a downward force due to surface tension Subsequently this vapor packet is pushed down towards the film. The vapor packet impinges on the horizontal surface The surface tension induced flow promotes the movement of pressure gradient driven impinging vapor packet towards the symmetric side walls The vapor turns upward near the side walls to initiate an identical bubble release cycle Similar patterns of bubble release were observed by Son and Dhir [23] in their axisymmetric simulations of saturated film boiling

Furthermore, the cyclic bubble release pattern can be discerned from Fig 4 4 and 4 5, which show the variation of space averaged wall heat flux with time for constant and variable thermal properties, respectively. For constant thermal properties (Fig 4 4), after an initial transient, we observed a cyclic pattern with the time period of 0 27 sec For variable thermal properties (Fig 4 5), we found a smaller time period of 0 23 sec Figure 4 6 shows the variation of interface heat flux with time for both the cases, namely, constant and variable thermal properties It can be observed that with the variable thermal properties, a higher magnitude of energy is transferred from vapor to liquid This energy is responsible for conversion of liquid into vapor Figure 4 7 shows the variation of fractional vapor volume (vapor volume/(vapor volume and liquid volume)) with time for both the cases Due to higher vapor generation, the bubble growth rate is faster for the case of variable thermal properties as compared with the constant thermal properties and thus, a smaller time period can be observed in the case of variable thermal properties. Son and Dhir [22] reported the bubble release time-period of the order of 0 1$\sim$0 15 seconds in

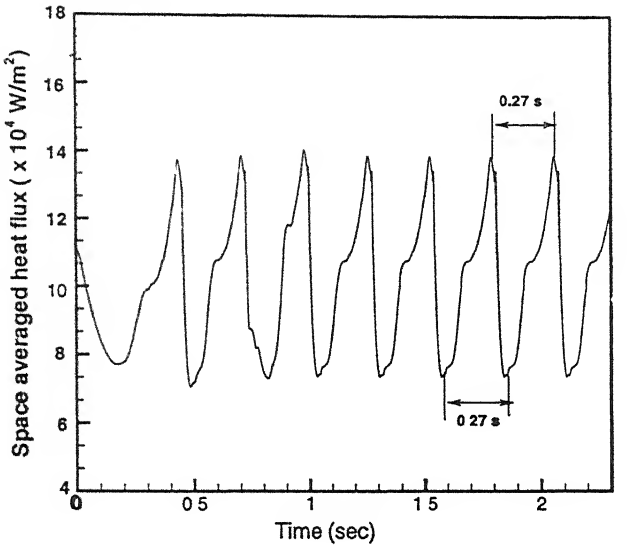

Figure 4 4. Fluctuation of space averaged heat flux on the wall surface with constant fluid thermal properties

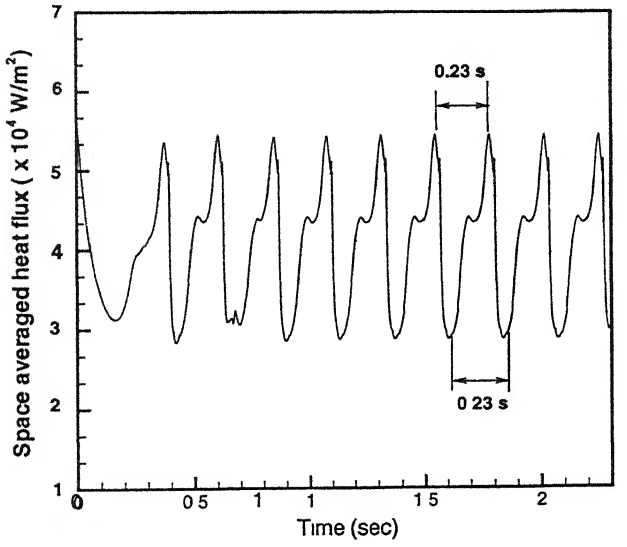

Figure 4 5: Fluctuation of space averaged heat flux on the wall surface with variable fluid thermal properties

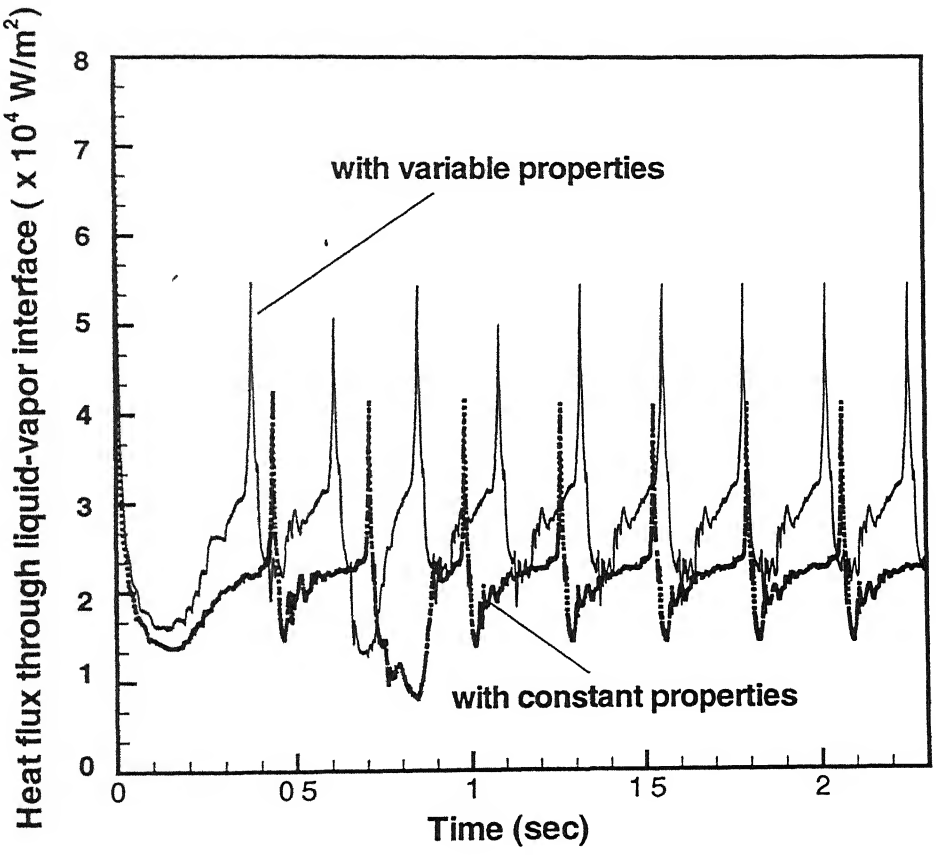

Figure 4 6 Fluctuation of liquid-vapor interface heat flux with time

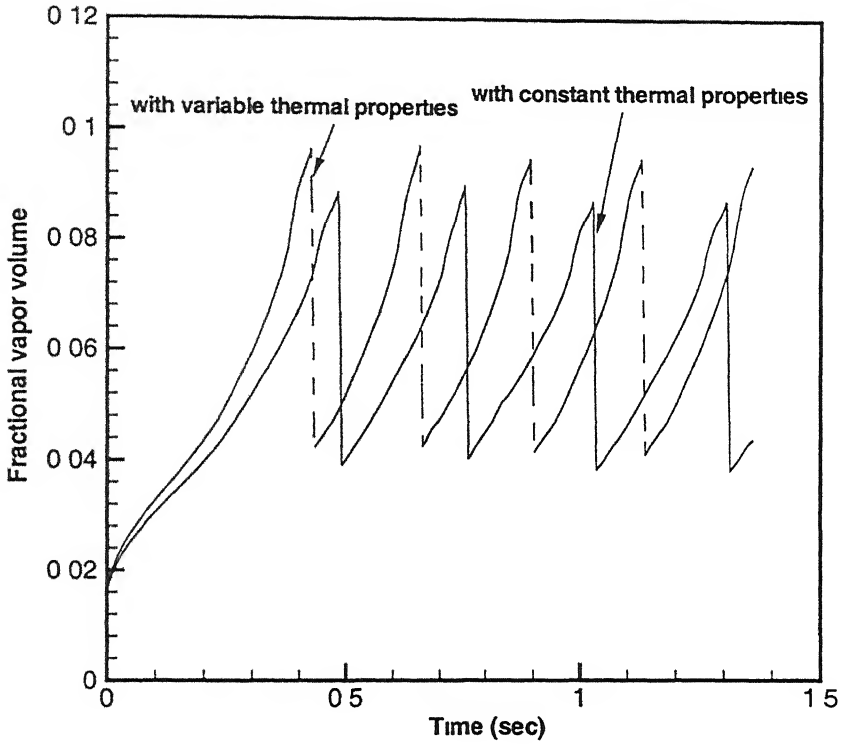

Figure 4 7· Variation of fractional vapor volume with time for constant and variable thermal properties

their numerical simulations using water at 1 atm pressure The simulations by Son and Dhir [22] were accomplished with the consideration of large degree of superheats, of the order of 100 C Since in the present work, the degree of superheat is 15° C, a relatively large time period is expected As mentioned earlier, the vapor generation is higher for the variable property simulation This observation is well supported by Fig 4 6 for heat flux through the liquid-vapor interface The interface area (in two-dimensional this is a curved line) is used for this calculation However, the wall heat flux (Figs 4 4 and 4 5) for constant properties is higher then that for the variable properties There is an apparent contradiction here This can be explained as the following Table 4 1 and 4 2 reveal that specific heat (c_p) of the constant property fluid is much higher than the average specific heat of the variable property fluid As the energy at any phase may be expressed in terms of the enthalpy (c_pT) of that phase, the temperature of the vapor at constant property is much less than that of the vapor at variable property The higher temperature of the vapor (for the case of variable property) sets up a higher temperature gradient at the interface entailing higher vapor generation.

Figures 4 8(a) and (b) show the isotherms and interfacial shape during the bubble growth at two different time instants Each isotherm almost follows the shape of the interface The spacing between the isotherms is in general uniform A deeper look into Fig 4 8(a) reveals slightly nonuniform distribution of the isotherms in the primary bubble In the primary bubble, the isotherms are a little closely spaced near the neck due to narrowing of the cross-sectional area and the upward motion of vapor

Figure 4 9 shows the temperature contours within the vapor film on the solid surface, near the location of minimum film thickness, for the degree of superheat 15° C The uniform spacing between the isotherms indicates that energy transfer from the wall, during film boiling, in this region, is governed primarily by conduction rather than convection This is further corroborated by Fig. 4 10, which shows the variation of peak heat flux value with the reciprocal of the minimum film thickness at various time instants The linear nature of variation indicates that heat flux is inversely proportional to vapor film thickness In addition, the nature of variation implies the dominance of conduction as mode of heat transfer near the location of the film with minimum thickness

Figures 4 11 and 4 12 show the velocity vectors at different arbitrary time instants, 0 375

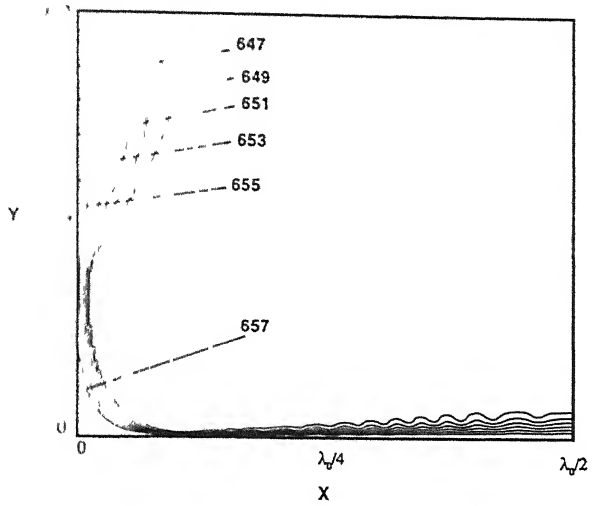

(a)

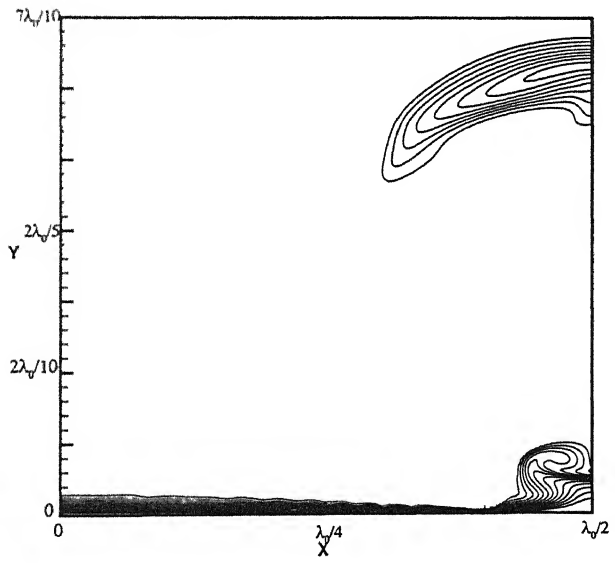

(b)

Figure 4 8 Isotherms for a superheat of $\Delta\theta = 15°C$ in the vapor over the computational domain at time instants 0 375 s and 0 625 s respectively In (b) contour levels are spaced at a temperature difference of $1°C$ for a range between $647 - 658°C$

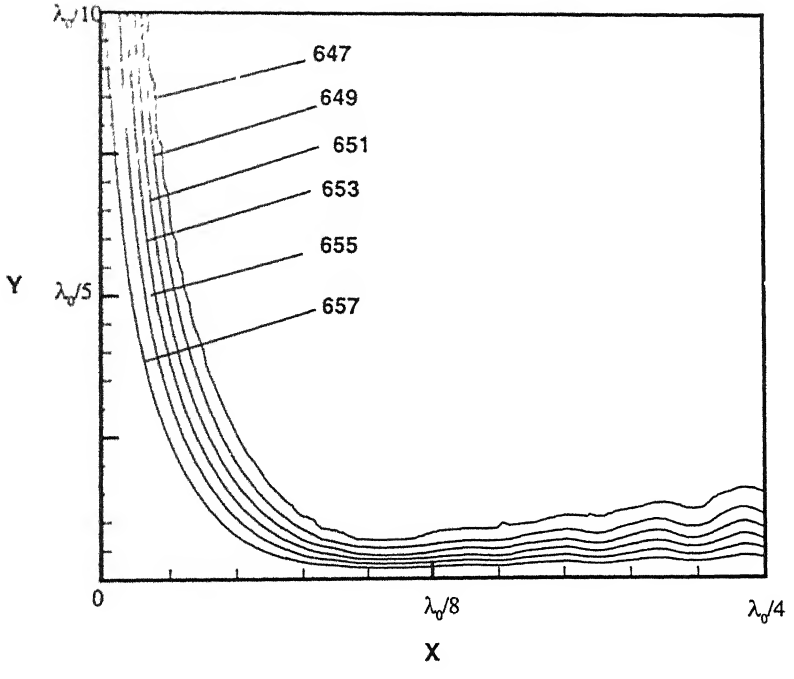

Figure 4.9 Isotherms for a superheat of $\Delta\theta = 15°C$ in an enlarged region of Fig 11(a) near the location of minimum film thickness

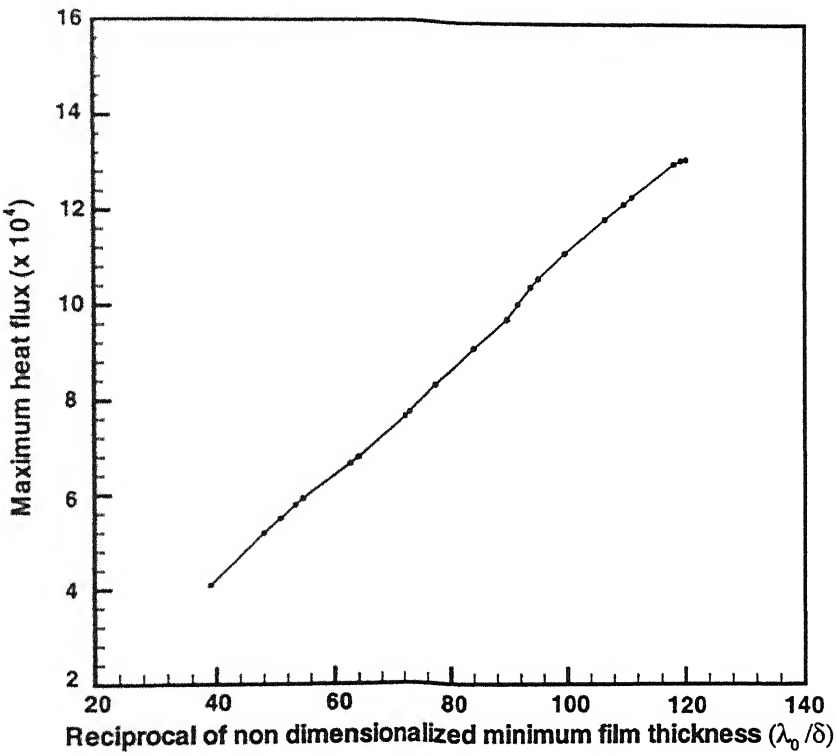

Figure 4 10 Variation of peak heat flux value with the reciprocal of minimum film thickness at various time instants

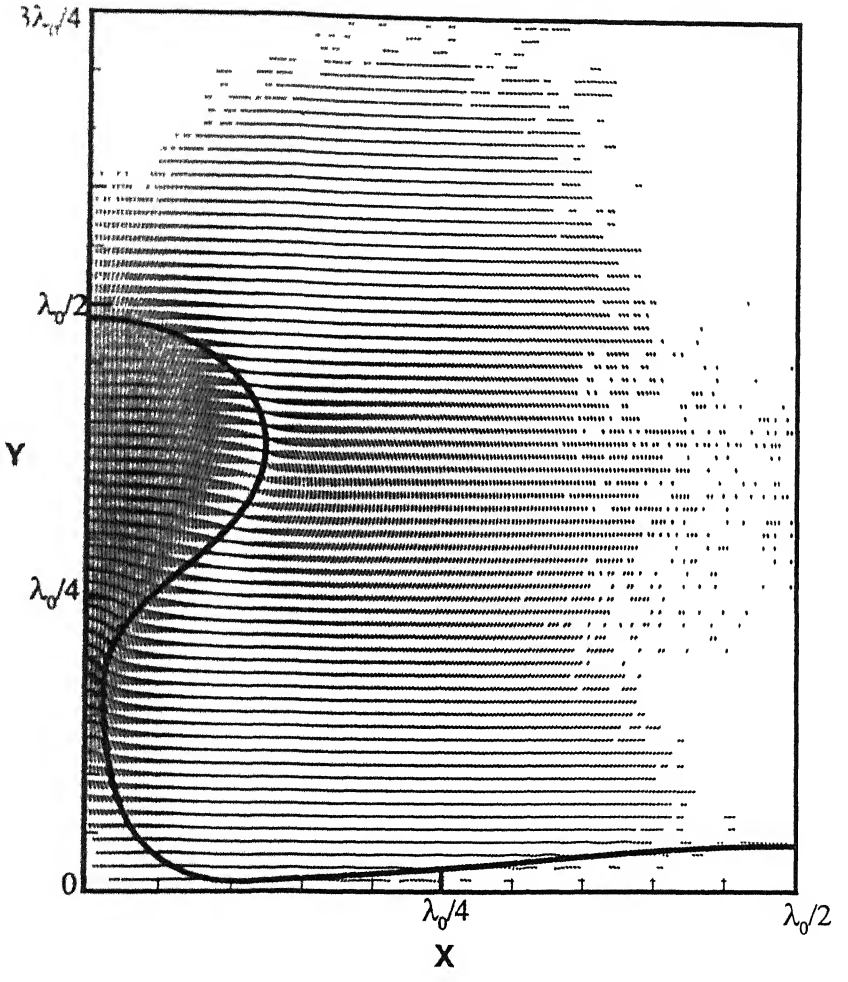

Figure 4.11· Velocity vectors for a superheat of $\Delta\theta = 15°$ at time = 0 375 s

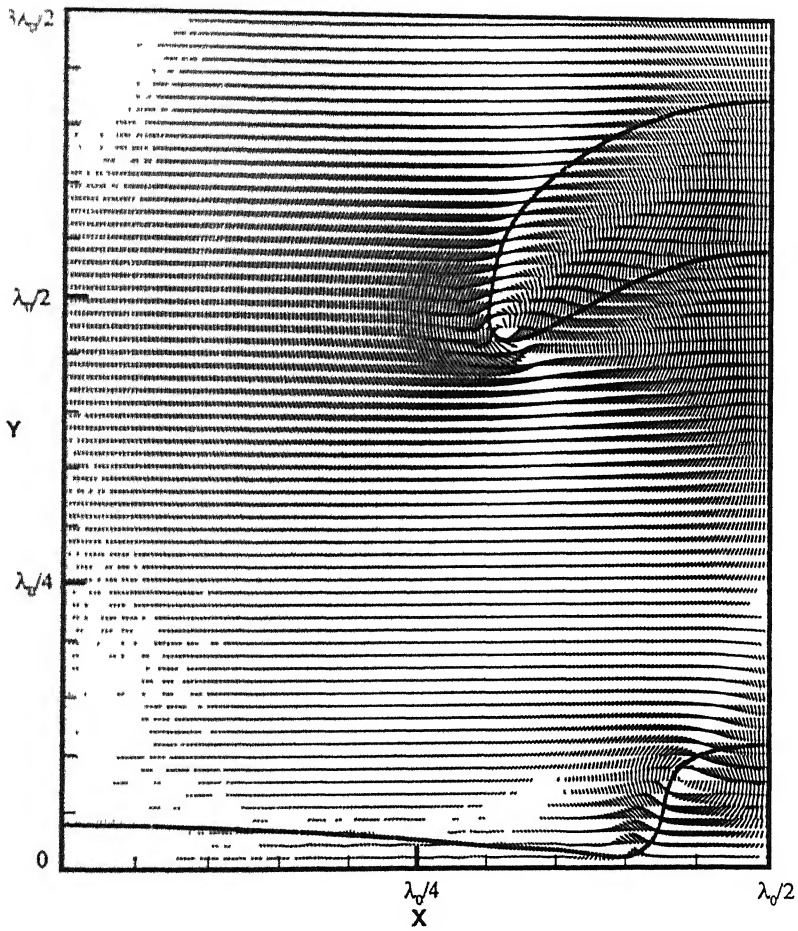

Figure 4.12: Velocity vectors for a superheat of $\Delta\theta = 15°$ at time = 0 625 s .

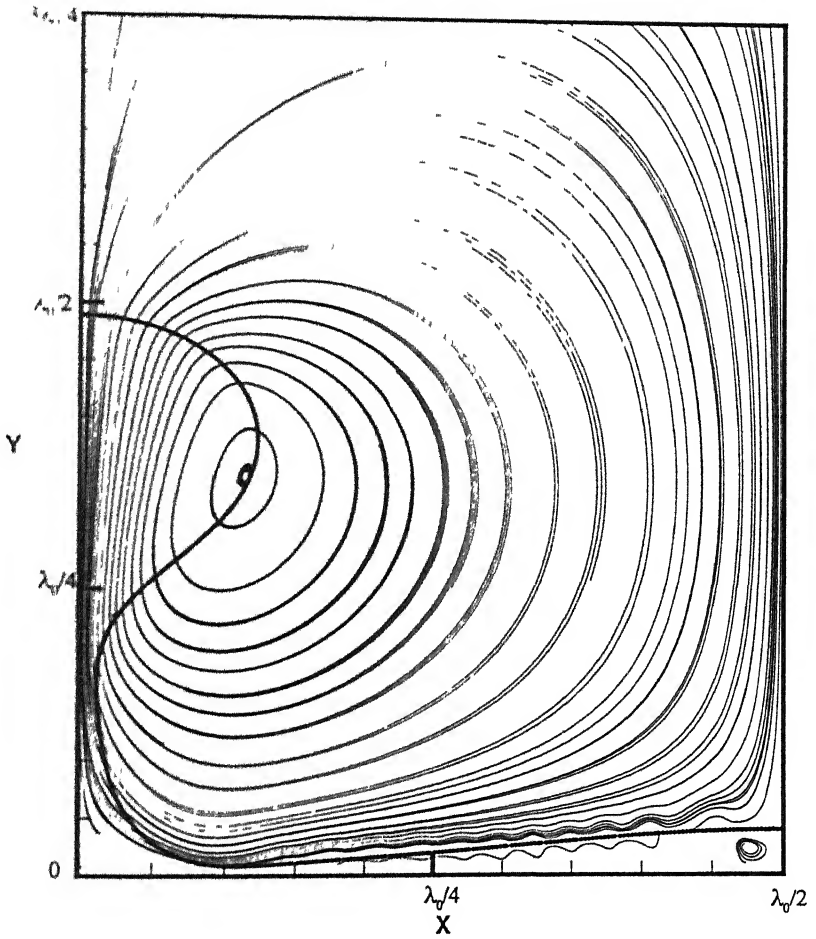

Figure 4 13. Streamlines at time = 0 375 s

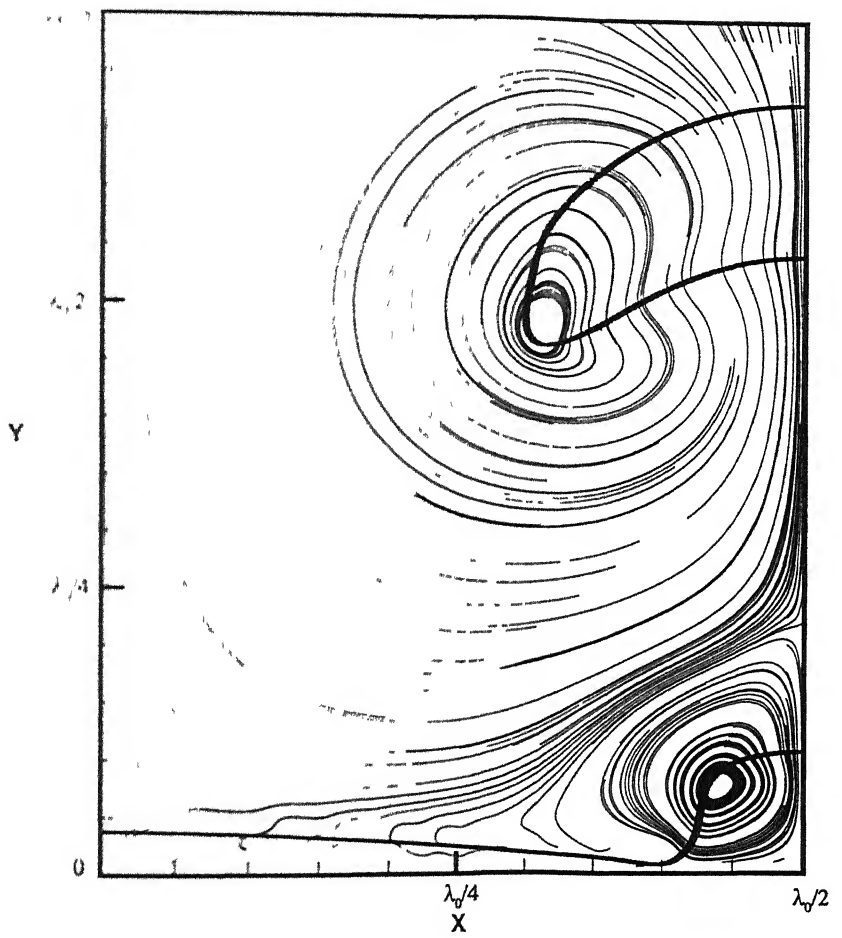

Figure 4 14 Streamlines at time = 0 625 s

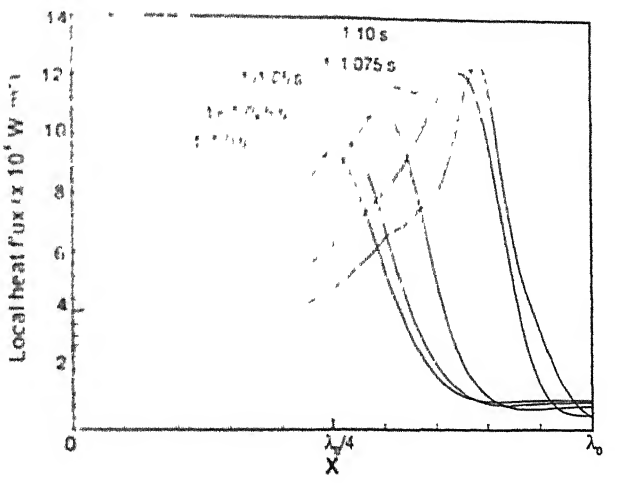

Figure 4 15 Variation of heat flux on the wall surface at various time instants before bubble release on right symmetric boundary

and 0 625 sec respectively, for the case of variable thermal properties of the vapor in the computational domain For clarity, velocity vectors are plotted at the alternative grid points It can be seen that the upward movement of the interface is much stronger in the primary bubble region (left side symmetric boundary in Fig 4 11) than in the region of secondary bubble (right side symmetric boundary in Fig 4 11) Figure 4 12 shows the velocity vectors just after the bubble has relased from right side symmetric boundary Furthermore, the vapor injected into the primary bubble through the thin film induces vortex motion near the interface which can be better observed in Figs. 4.13 and 4 14 Such observations are quite similar to what have been found by Son and Dhir [22]

The most important quantitative issue of film boiling is the wall heat transfer Although the wall temperature is constant in the present simulation, the heat flux from the wall varies over the wall surface. Figure 4 15 shows the distribution of wall heat flux for 15°C superheat at various time instants. We observe that the profile of the heat flux distribution at a particular instant is just reciprocal to that of the vapor film thickness at that instant The heat flux from the surface is inversely proportional to the vapor film thickness at any wall location. Maximum heat transfer takes place at the location where the film is thinnest Under the bubble core, very little heat transfer takes place It is evident that the maximum and minimum heat flux corresponds to minimum and maximum vapor film thickness, respectively. We observe the magnitude of the peak heat flux to increase

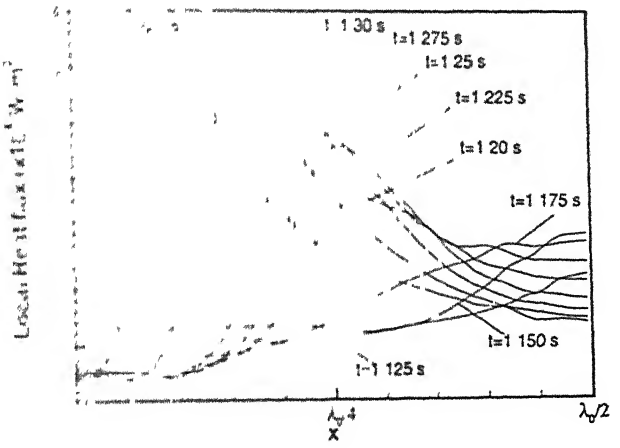

Figure 4 16 Variation of heat flux on wall surface at time instants after the bubble release on right symmetric boundary

in passage of time. Consequently, the peak shifts to the right. The figure signifies growth of a bubble at the right symmetric plane. This can be explained in the following way As the bubble grows, i.e., the interface in the peak region moves upward, the interface at other regions fails to conserve the vapor volume. The vapor generation is unable to offset the conservation of vapor volume by a large magnitude. Thus the film thickness is reduced over most of the wall surface except the region just underneath the bubble core Furthermore, the location at which the film is the thinnest, moves radially inward (considering the projection of the spherical bubble is circular) on the solid surface as the interface evolves into a fully grown bubble The radially inward movement of the thinnest layer explains the shift of the peak

Further, Fig. 4 16 shows the same trend in spatial heat flux variations for time instants after the bubble release at the right symmetry boundary, with peak heat flux shifting near to left symmetry boundary. We observe that there is sudden decrease in peak heat flux value just after the bubble release. The space averaged Nusselt number at the solid-fluid interface can be defined as the nondimensional heat flux (*or* temperature gradient) at the wall in the following way

$$\overline{\mathrm{Nu}} = \frac{2}{\lambda_o} \int_0^{\lambda_o/2} \frac{\lambda}{(\theta_w - \theta_{sat})} \left.\frac{\partial \theta}{\partial y}\right|_{y=0} dx \qquad (4\,2)$$

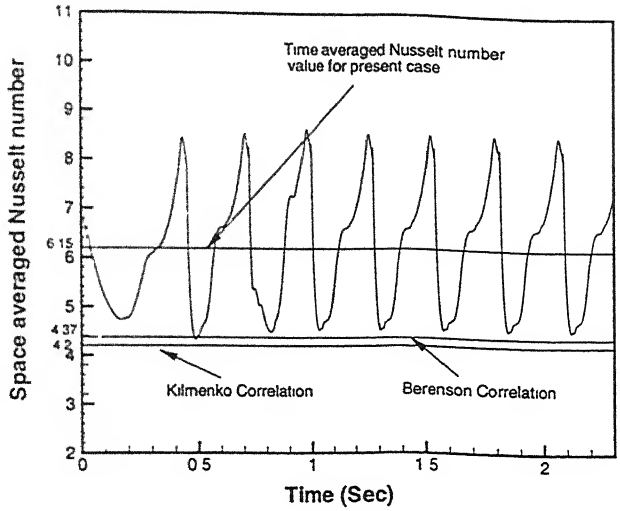

Figure 4 17 Nusselt number variation with time (with constant thermal properties)

where λ is the characteristic length Figures 4 17 and 4 18 show the evolution of the space averaged Nusselt number with time on the horizontal surface for constant and variable thermal properties, respectively A cyclic temporal variation (initial transients upto three cycles being ignored) of the space averaged Nusselt number has been observed We note that during the stage of bubble growth, the space averaged Nusselt number increases As the interface in the peak region moves upward, the vapor film at another location of wall becomes extremely thin and thereby entails enhanced heat transfer Just after the departure of the bubble, the heat transfer rate decreases leading to a sudden drop in Nusselt number which can be seen in the plot This is because the surface tension, acting as a restoring force, pulls down the interface at the location of the peak, and in turn, the interface in the valley region moves upward Thus the average film thickness over the major portion on the surface increases leading to a reduction in heat transfer Thereafter, as the next bubble again starts growing, the Nusselt number increases and this cycle repeats

Now we compare our time and space averaged Nusselt number values with the predictions made in earlier investigations The correlations due to Berenson [2] depict the Nusselt numbers constant with time and are not affected by the bubble dynamics unlike the

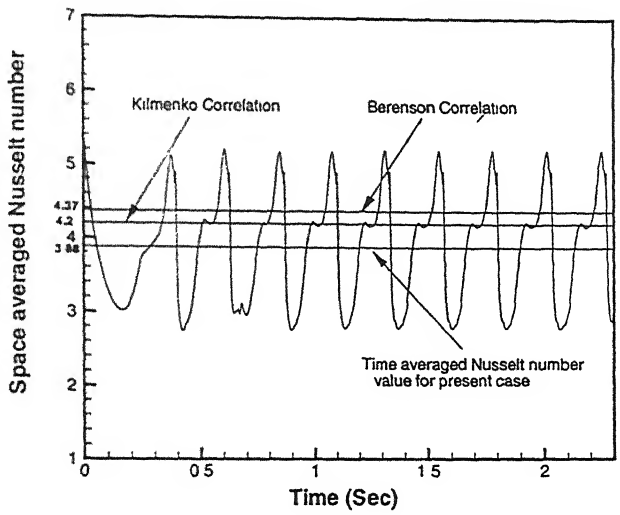

Figure 4.18 Nusselt number variation with time (with variable thermal properties)

present numerical results. Berenson [2] has predicted the Nusselt number as

$$\mathrm{Nu} = 0.42 \left\{ \frac{\mathrm{Gr}\ \mathrm{Pr}}{\beta} \right\}^{1/4} \tag{4.3}$$

Here Gr and Pr are the Grashof number and Prandtl number, respectively, defined by

$$\begin{aligned} \mathrm{Gr} &= \frac{\rho_g^2 g \lambda^3}{\mu_g^2} \left(\frac{\rho_l}{\rho_g} - 1 \right) \\ \mathrm{Pr} &= \frac{c_{P_g} \mu_g}{k_g} \end{aligned} \tag{4.4}$$

and β is the ratio of sensible heat to latent heat described as

$$\beta = \frac{c_{P_g} \Delta\theta}{h_{fg}} \tag{4.5}$$

Klimenko [12] carried out a somewhat generalized analysis of film boiling on horizontal flat plates Employing a basic formulation, similar to that Berenson [2], Kilmenko developed a correlation that included data near critical pressure similar to the present numerical study According to his correlation, Nusselt number data for film boiling on an

upward facing horizontal surface was expressed with in ±25 percent as

$$Nu = 1.90 \times 10^{-1} Gr^{1/3} Pr^{1/3} f_1, \quad \text{for } Gr < 4.03 \times 10^5 \tag{4.6}$$

$$Nu = 2.16 \times 10^{-2} Gr^{1/2} Pr^{1/3} f_2, \quad \text{for } Gr > 4.03 \times 10^5 \tag{4.7}$$

where,

$$f_1 = 1. \quad \text{for } \beta > 0.71$$
$$= 0.89\beta^{-1/3} \quad \text{for } \beta < 0.71$$
$$f_2 = 1 \quad \text{for } \beta > 0.50$$
$$= 0.71\beta^{-1/3} \quad \text{for } \beta < 0.50$$

In Figs. 4.17 and 4.18 we compare the span average Nusselt numbers caluculated with constant and variable thermal properties to the correlations of Berenson (Eq. 4.3) and Klimenko (Eq. 4.5 and 4.6). Equation 4.4 implicitly calculates the Nusselt number with the characteristic length and the thermal conductivity of the vapor evaluated at the wall temperature. The correlations of Berenson and Klimenko both specify that the properties be taken at average film temperature ($(T_{wall}+T_{sat})/2$). The time-space average Nusselt numbers for both simulations and both correlations are listed in Table 4.4, from which it can be seen that there is reasonable agreement between all four values but the simulation with variable properties is closer to the correlations. If the properties in the correlations are evaluated at the wall temperature, the Nusselt numbers for Berenson and Klimenko become 4.80 and 4.36 respectively. This illustrates the shortcomings of attempts to account for the rapid variation in the fluid properties very near the critical point by evaluating them at a single temperature, whether in a correlation or a simulation. The simulation with variable properties takes proper account of their nonlinear variation and defines the Nusselt number in a rational manner. The discrepancies in the results between the values due to correlations and present analysis could also be attributed to the existence of wavelength shorter than the *most dangerous* wavelength as observed in the experiments of Hosler and Westwater [10]. As also noted by Son and Dhir [22], this difference could be due to the inability of a two-dimensional model to take into account the additional variations pertaining to the interface position. Such variations are expected

to provide more efficient flow patterns for vapor removal and thus enhanced heat transfer

Case	Nu (computed)	Nu (Berenson model)	Nu (Klimenko correlation)	% variation from Berenson	% variation from Klimenko
with variable thermal properties	3 88	4 37	4 20	= − 11 2	= − 7 6
with constant thermal properties	6 15	4 37	4 20	= + 40 7	= + 46 4

Table 4 4 Comparison of predicted Nusselt number with that of Berenson and Klimenko correlation for constant and variable thermal properties

Chapter 5

Conclusion and Scope for Future Work

Investigations of pool boiling have been carried out with the aim to employ numerical techniques to advance the understanding of bubble formation and the induced fluid motions and consequently their influence on the instantaneous heat transfer characteristics from the wall surface This numerical investigation provided a nice insight into bubbly film boiling flows, yielding fascinating results The results of this work revealed

- Successful predictions of bubble growth and heat transfer characteristics for film boiling on a horizontal surface using VOF method

- The predictions have revealed unsteady periodic nature of bubble growth at the nodes and the anti-nodes

- Film thickness and heat transfer coefficient are found to vary spatially and temporally during the growth of interface

- Magnitude and location of maximum heat transfer from the wall surface are found

to be dependent on the magnitude and location of minimum film thickness

- The Nusselt numbers for film boiling (with variable thermal properties) obtained in the present work are only 11.2% and 7.6% lower than those obtained from Berenson's model and Klimenos correlation respectively

In the present work, the computations were performed under two-dimensional and symmetric boundary conditions using a predefined separation between regions of bubble formation. In future computations, the restrictive assumption of boundary conditions will be relaxed and a fully three-dimensional prediction must be aimed for. Future plans also include the use of our method in numerical studies of the transition region of the boiling curve, in which the problems associated with moving contact line will be addressed

References

[1] Banerjee D and Dhir, V K , Study of Subcooled Film Boiling on a Horizontal Disk part I-Analysis, *Journal of Heat Transfer*, Vol 123, pp 271-284, 2001

[2] Berenson, P J , Film-Boiling Heat Transfer from a Horizontal Surface, *Journal of Heat Transfer*, Vol 83, pp 351-358, 1961

[3] Brackbill, J U , Kothe, D B and Zemach, C , A Continuum Method for Modeling Surface Tension, *Journal of Comput Phys* , Vol 100, pp 335-354, 1992

[4] Carey P Van, *Liquid-Vapor Phase Change Phenomena*, Series in Chemical and Mechanical Engineering, Taylor and Francis, 1992

[5] Chang, Y C , Hou, T Y , Merriman, B and Osher, S , A Level Set Formulation of Eulerian Interface Capturing Methods for Incompressible Fluid Flows, *Journal of Comput Phys* , Vol 124, pp 449-464, 1996

[6] Colella, P , and Woodward, P , The Piecewise Parabolic Method for Gas Dynamical Simulation,*Journal of Comput Phys* , Vol 54, pp 174-201, 1984

[7] Dhir, V K , Numerical Simulations of Pool-Boiling Heat Transfer, *AIChE Journal*, Vol 47, pp 813-834, 2001

[8] Harlow, F. H. and Welch, J. E., Numerical Calculation of Time-Dependent Viscous Incompressible Flow of Fluid with Free Surface, *Phys. Fluids*, Vol. 8, pp. 2182-2189, 1965.

[9] Hirt, C. W. and Nichols, B. D., Volume of Fluid (VOF) Method For the Dynamics of Free Boundaries, *Journal of Comput. Phys.*, Vol. 39, pp. 201-225, 1981.

[10] Hosler, E. R., and Westwater, J. W., Film Boiling on a Horizontal Plate, *ARS J.*, Vol. 32, pp. 553-560, 1962.

[11] Juric, D. and Tryggvason, G., Computation of Boiling Flows, *Int. Journal Multiphase Flow*, Vol. 24, pp. 387-410, 1998.

[12] Klimenko, V., Film Boiling on a Horizontal Plate-New Correlation, *International Journal of Heat Transfer*, Vol. 24, pp. 69-79, 1981.

[13] Kothe, D. B., Rider, W. J., Mosso, S. J., Brock, J. S. and Hochstein, J. I., Volume Tracking of Interface Having Surface Tension in Two and Three Dimensions, *AIAA Paper 96-0859. Presented in the 34th Aerospace Science Meeting and Exhibit, Reno, NV*, Jan. 15-18, 1996.

[14] Leonard, B. P., A Stable and Accurate Convective Modelling Procedure Based on Quadratic Upstream Interpolation, *Comput. Methods Appl. Mech. Engg.*, Vol. 57, pp. 415-438, 1979.

[15] Noh, W. F., and Woodward, P. R., SLIC (Simple Line Interface Method), *Lacture Notes in Physics*, Vol. 59, pp. 330-340, 1976.

[16] Osher, S., and Sethian, J. A., Front Propagating with Curvature-Dependent Speed Algorithms Based on Hamilton-Jacobi Formulation, *Journal of Comput. Phys.*, Vol. 79, pp. 12-49, 1988.

17 Puckett E G Almgren A S, Bell, J B, Marcus, D L and Rider, W J, A High Order Projection Method for Tracking Fluid Interface in Variable Density Incompressible Flows, *Journal of Comput Phys*, Vol 130, pp 269-282, 1997

18 Puckett E G and Saltzman, J S, A 3D Adoptive Mesh Refinement Algorthim for Multimaterial Gas Dynamics, *physica D*, Vol 60, pp 84-93, 1992

[19] Rider, W J, and Kothe, D B, Stretching and Tearing Interface Tracking Methods Technical report AIAA 95-1717 AIAA (1995) *Presented at the 33rd Aerospace Sciences Meeting and Exhibit, Reno, NV*,1995

[20] Rider, W J and Kothe, D B, Reconstructing Volume Tracking, *Journal of Comput Phys*, Vol 141, pp 112-152, 1998

[21] Rudman M, Volume-Tracking Methods for Interfacial Flow Calculations, *Int Journal Numer Methods Fluids*, Vol 24, pp 671-691, 1997

[22] Son, G and Dhir, V K, Numerical Simulation of Saturated Film Boiling on a Horizontal Surface, *Journal of Heat Transfer,* Vol 119, pp 535-533, 1997

[23] Son, G and Dhir, V K, Numerical Simulation of Film Boiling Near Critical Pressures with a Level Set Method, *Journal of Heat Transfer,* Vol 120, pp 183-192, 1998

[24] Sussman, M, Smereka, P and Osher, S, A Level Set Approach for Computing Solutions to Incompressible Two-Phase flow,, *Journal of Comput Phys*, Vol 114, pp 146-159, 1994

[25] Unverdi, S O and Tryggvason, G, A front-tracking method for viscous, incompressible, multi-fluid flows, *Journal of Comput Phys*, Vol 100, pp 25-37, 1992

[26] Van der Vorst, H A, Bi-CGSTAB A Fast and Smoothly Converging Variant of Bi-CG for Solution of Non-Symmetric Linear Systems, *SIAM J Sci Stat Comput*,

Vol 12, pp 631-644, 1992

[27] Welch S W J , Direct Simulation of Vapor Bubble Growth, *Int Journal of Heat and Mass Transfer*, Vol 41, No 12, pp 1655-1666, 1998

[28] Welch, S W J and Rachidi, T , Numerical Computation of Film Boiling Including Conjugate Heat Transfer, *Numerical Heat Transfer B*, Vol 42, pp 35-53, 2002

[29] Welch, S , Trapp, J and Mortensen, G , Interface Tracking in Two-Phase Flow Simulations Using a Simple Subgrid Counting Procedure, *Numerical Methods in Multiphase Flows*, FED-Vol 185, pp 293-299, 1994

[30] Welch, S W J and Wilson, J , A Volume of Fluid Bases Method for Fluid Flows with Phase Change, *Journal of Comput Phys* , Vol 160, pp 662-682, 2000

[31] Youngs, D L , Time-Dependent Multi-Material Flow with Large Fluid Distortion in K W Morton and M J Baines(eds.), *Numerical Methods for Fluid Dynamics*, Academic Press, New York, pp 273-285, 1982

Appendix A

A.1 List of Subroutines

film.f - main program this calls all subroutines

bc.f - boundary conditions

delta.f - calculates dx,dy (cell size)

density.f - calculates new density field (equation 3 26)

energy.f - bulk phase energy equation (equation 3 23)

property.f - After each iteration (in energy f) with the help of temperature value at the center of the cell This subroutine calculates thermal conductivity and specific heat for each cell Here we used a data set of thermal properties (From NBS/NRC Table) containing 10 values at a range of 15 C superheat and interpolated it to get intermediate values at any temperature corresponding to cell center

iface.f - interface reconstruction with the help of LVIRA algorthim

indta.f - input data and also calculates normalization constant for kernel function

init.f - initial conditions

iters.f - bcgstab routine and supporting routines

junpro.f - This subroutine computes explicit junction voids The junction voids are used for density and viscosity terms in the momentum equations

lgvol f - calculates volume of liquid and vapor in an interface cell

linseg f - returns the intersection points of the interface with the cell boundaries

movelt.f - sets phase of each cell after the calculation of new density field

outdta f - outputs data to data files

pviter.f - builds modified continuity equation that includes mass source terms and calls iteration routine

qint.f - This programme finds temperature of a 2-phase cell based on extrapolation and also determines the interfacial heat fluxes For calculation of interfacial heat flux terms (sourcv and sourcl), we requires exact value of thermal conductivity along the line joining from midpoint of linear interface of a cell (i,j) to the center of neighboring cell (iq,jq) qint f calls a subroutine named point f for the calculation of exact value of thermal conductivity

point.f - This subroutine finds out the point of intersection of the cell faces and the line that conects the center of the cell (iq,jq) with the mid point of phase interface Then, with the use of thermal resistance concept, equivalent thermal conductivity along this line is calculated, which is used in qint f for the calculation of the source terms

setup.f - initialize velocities and other cell variables and also sets the initial interface profile

smooth.f - smoothing of void field with kernel function calculation (Eqn 3 19-3 22)

solid.f - solution of energy equation in adjacent solid surface However, in the present simulation we set wall temperature in this subroutine

vexplt.f - momentum equations (Eqn 3 25)

weight.f - weightings for smoothed gradient calculation

A.2 Flow Chart

FLOW CHART

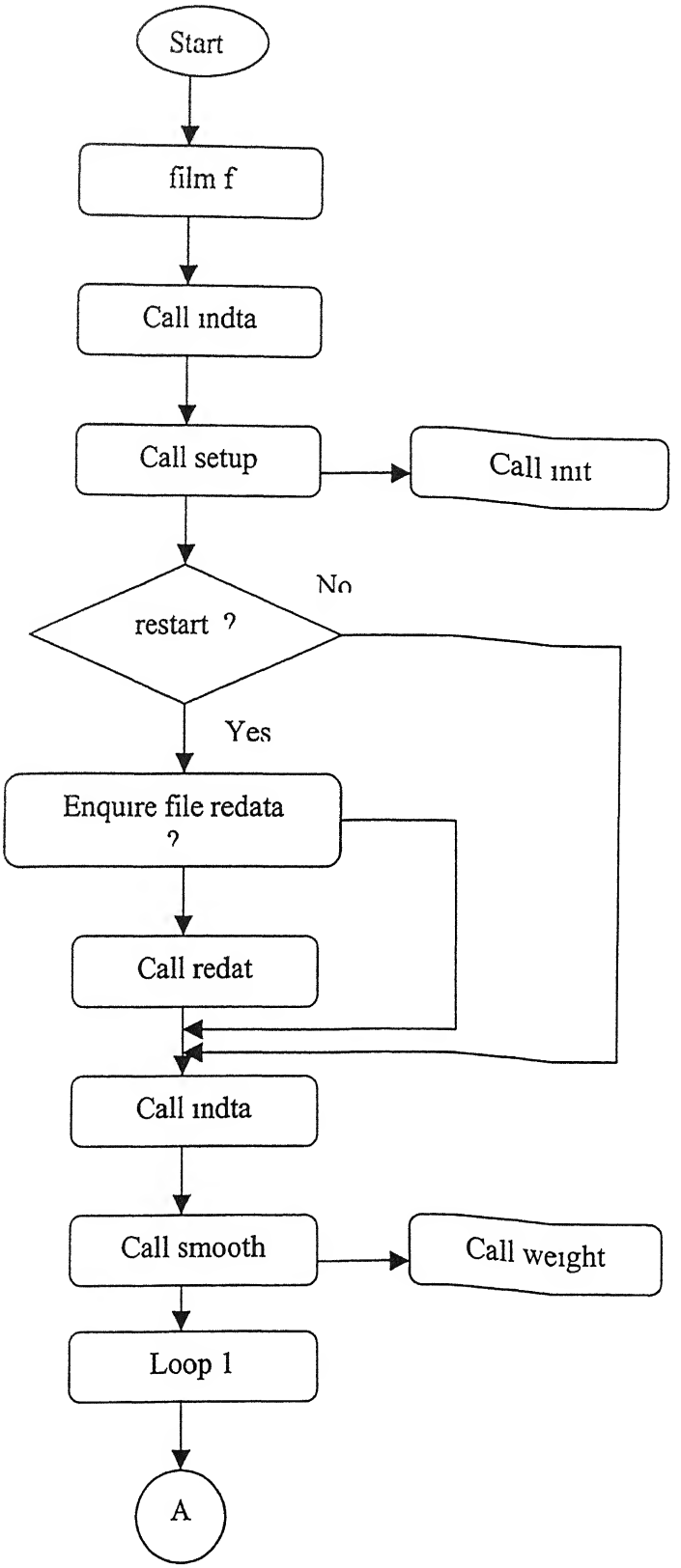
Start
film f
Call ındta
Call setup
Call ınıt
restart ?
No
Yes
Enquire file redata ?
Call redat
Call ındta
Call smooth
Call weight
Loop 1
A

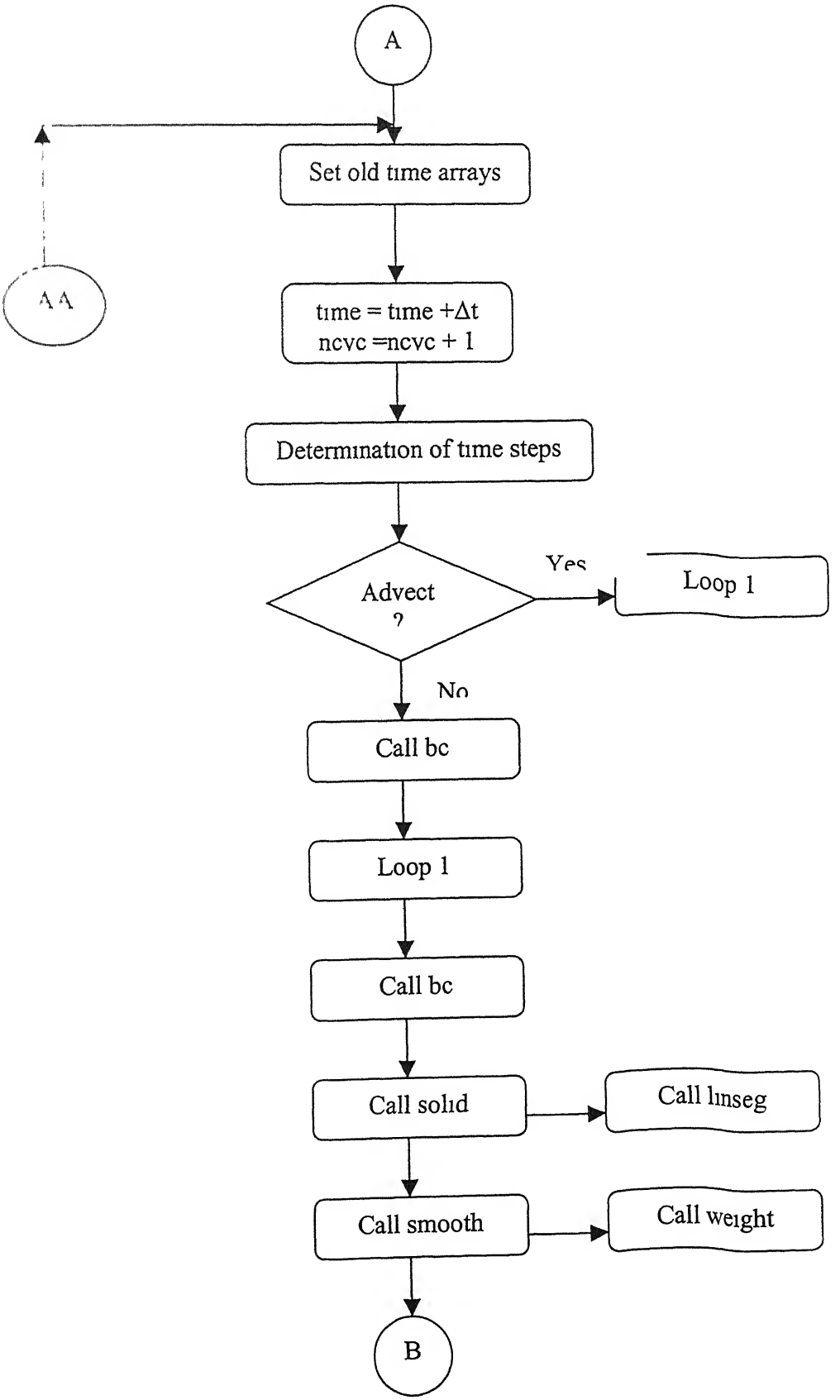
A
Set old time arrays
AA
time = time +Δt
ncyc =ncyc + 1
Determination of time steps
Advect
?
Yes
Loop 1
No
Call bc
Loop 1
Call bc
Call solid
Call linseg
Call smooth
Call weight
B

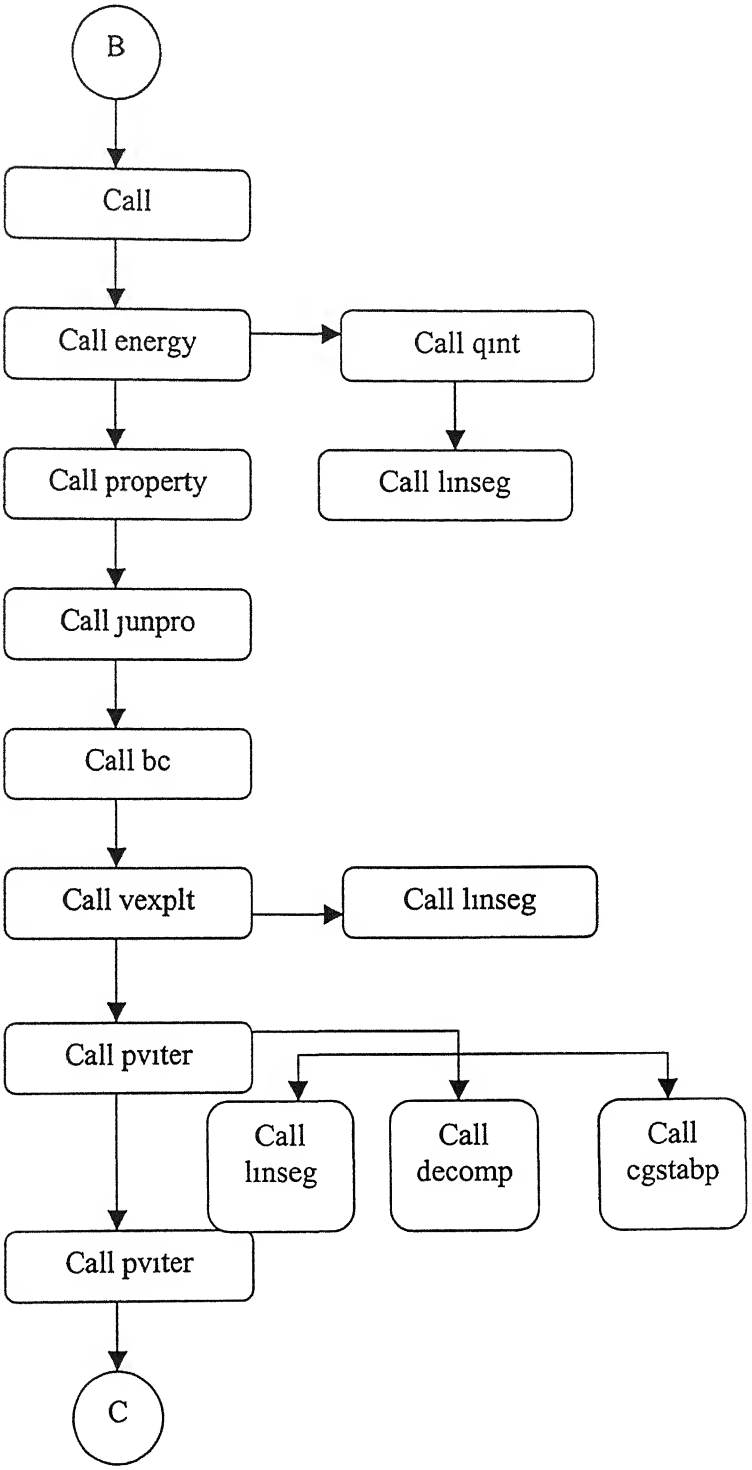
B
Call
Call energy
Call qint
Call property
Call linseg
Call junpro
Call bc
Call vexplt
Call linseg
Call pviter
Call linseg
Call decomp
Call cgstabp
Call pviter
C

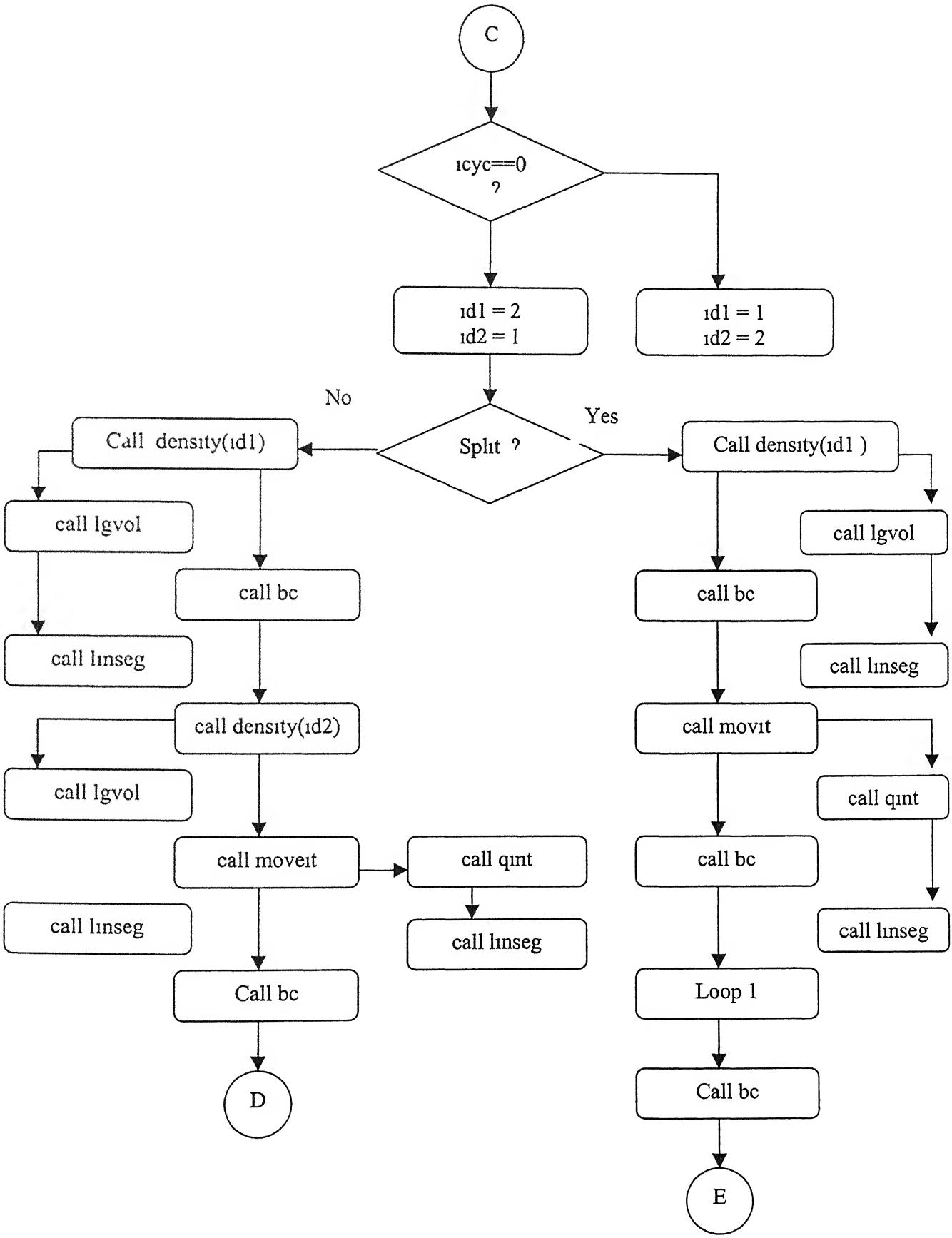
C
icyc==0 ?
id1 = 2
id2 = 1
id1 = 1
id2 = 2
No
Yes
Split ?
Call density(id1)
Call density(id1)
call lgvol
call bc
call linseg
call density(id2)
call lgvol
call moveit
call qint
call linseg
Call bc
D
call lgvol
call bc
call linseg
call movit
call qint
call bc
call linseg
Loop 1
Call bc
E

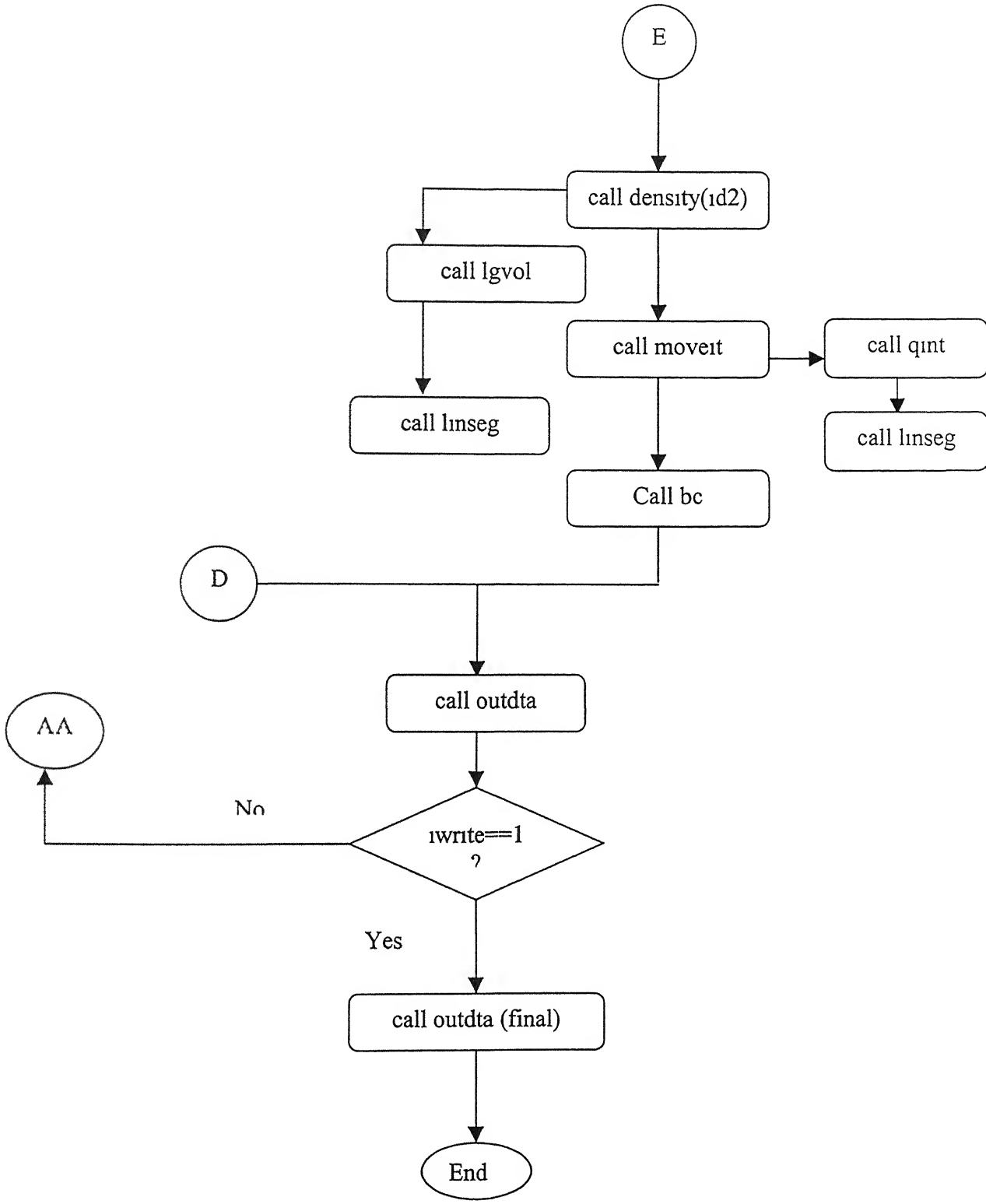
E
call density(id2)
call lgvol
call moveit
call qint
call linseg
call linseg
Call bc
D
call outdta
AA
No
iwrite==1
?
Yes
call outdta (final)
End

LOOP - 1

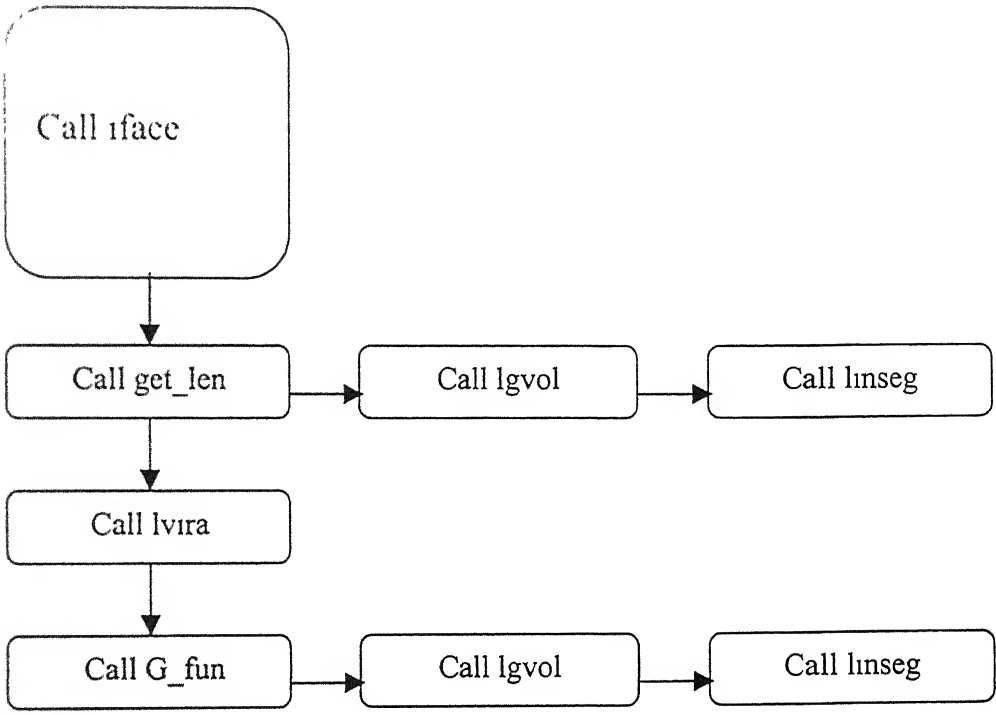
Call iface
Call get_len
Call lgvol
Call linseg
Call lvira
Call G_fun
Call lgvol
Call linseg